A System for Obstacle Detection During Rotorcraft Low Altitude Flight

BIR BHANU, Fellow, IEEE
SUBHODEV DAS, Member, IEEE
BARRY ROBERTS
DAVE DUNCAN
Honeywell Systems and Research Center

An airborne vehicle such as a rotorcraft must avoid obstacles like antennas, towers, poles, fences, tree branches, and wires strung across the flight path. Automatic detection of the obstacles and generation of appropriate guidance and control actions for the vehicle to avoid these obstacles would facilitate autonomous navigation. The requirements of an obstacle detection system for rotorcraft in low-altitude Nap-of-the-Earth (NOE) flight based on various rotorcraft motion constraints is analyzed here in detail. It argues that an automated obstacle detection system for the rotorcraft scenario should include both passive and active sensors to be effective. Consequently, it introduces a maximally passive system which involves the use of passive sensors (TV, FLIR) as well as the selective use of an active (laser) sensor. The passive component is concerned with estimating range using optical flow-based motion analysis and binocular stereo. The optical flow-based motion analysis that is combined with on-board inertial navigation system (INS) to compute ranges to visible scene points is described. Experimental results obtained using land vehicle data illustrate the particular approach to motion analysis.

Manuscript received May 10, 1993; revised March 11, 1995.

IEEE Log No. T-AES/32/3/05862.

This work was supported by NASA under Contract NAS2-12800 at Honeywell Systems and Research Center.

Authors' current addresses: B. Bhanu and S. Das, College of Engineering, University of California, Riverside, CA 92521-0425; B. Roberts and D. Duncan, Honeywell Systems and Research Center, 3660 Technology Dr., Minneapolis, MN 55418.

I. INTRODUCTION

In recent years, considerable effort has been put toward the detection of obstacles that present themselves to ground vehicles. Using primarily active sensors, such as a laser scanner, obstacles (like fence posts, rocks, and vegetation) within the field-of-view (FOV) of the vehicle's sensor are detected [21, 48]. Passive sensors such as a TV camera are also being used to detect obstacles for ground vehicles [14, 24]. However, little work has been done for the detection of obstacles for a rotorcraft performing a low-altitude flight [19, 33, 34, 38, 46, 47, 49]. For both commercial and military rotorcraft flying at low altitudes, obstacles result in numerous accidents [50]. *Obstacles*, in the context of a rotorcraft, are defined as physical objects (natural or man-made) that present a danger of collision to the rotorcraft. Examples of obstacles are antennas, towers, poles, fences, tree branches, wires strung across the flight path, etc. In contrast, *hazards* are situations that expose the rotorcraft to danger or adversely affect the mission in some other way. Examples of hazards are fire, wind, rotor down wash, haze, fog, precipitation, etc. Automatic detection of obstacles and their display to the pilot and/or automatic guidance and control actions triggered by such detection, would help conserve the pilot's attention for the mission tasks, thus contributing to mission success and, most importantly, saving lives. The problem of obstacle detection is especially serious in a single-pilot rotorcraft where the pilot's attention must be concentrated on mission tasks.

During terrain flight, military rotorcraft use surrounding vegetation, terrain, and man-made objects to conceal themselves from the visual or electronic detection systems by flying close to the Earth's surface. There are three broad categories of rotorcraft flight [27]: low-level, contour, and Nap-of-the-Earth (NOE) flight. These are illustrated in Fig. 1. During *low-level flight*, a constant speed and altitude are maintained of the rotorcraft. During *contour flight* a rotorcraft undergoes considerable variations in altitude and air speed. During *NOE flight* a rotorcraft flies as close to the Earth's surface as vegetation or other obstacles permit. Among these three categories, NOE flight is the most demanding on the pilot. During NOE flight, air speed (0 to 40 kt) and altitude (under 100 ft) vary according to terrain, weather, and ambient light. Commercial rotorcraft share most of the same obstacles and hazards of low-level and contour flight with military rotorcraft. Rescue, fire fighting, police helicopters as well as medicopters all must fly into and out of areas where numerous obstacles to air navigation exist. All these services could benefit from a means of detecting the presence of obstacles in the flight path. Poor visibility due to weather conditions, time of day, and terrain can hinder the pilot's knowledge of obstacles and hazards, and risk the safety of the helicopter and its passengers [4].

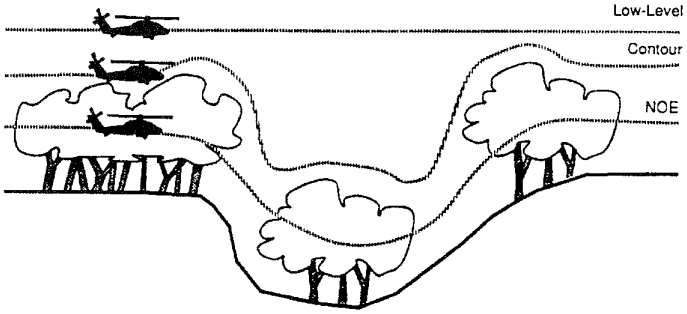

Fig. 1. Three broad categories of rotorcraft flight: low-level, contour, and NOE flight.

Presently, rotorcraft crew members rely on a sophisticated combination and fusion of sensors, "smart skin" antennas, computers, and displays in order to accomplish their mission under conditions of darkness, reduced visibility, bad weather, or NOE operations in a hostile environment. The state-of-the-art in NOE rotorcraft flight involves the use of forward looking infrared (FLIR) imagery for the copilot and some kind of night vision goggles for the pilot. The pilot manually flies the rotorcraft with flight path planning assistance from the copilot.

In principle, the problem of obstacle detection for rotorcraft navigation can be completely solved if either the range map to all points in front of the rotorcraft is supplied, or the image acquired at each instant of time can be segmented, recognized into its constituent parts such as sky, poles, trees, river, and the ranges to these parts are given. In fact, if the range from the known sensor location to each object point within a certain region of space close to the flight path were given, then a solution to the obstacle detection problem would have been obtained easily. The individual range values together with the rotorcraft velocity would yield the time-of-impact for the different points, the points with small time-of-impact values could be identified as belonging to potential obstacles. Thus, automated NOE flight capability, which will relieve the pilot's work load and will allow single pilot missions, requires, 1) a sensor suite that is able to map out the region ahead of the rotorcraft, determining the obstacles that are of concern; 2) a trajectory generation algorithm that defines the optimum flight path through that region considering threats, way points, and other constraints; and 3) a flight control system that guarantees maneuverability, stability, and robustness. However, the design of a sensor system that could be used for dynamic range mapping of the region ahead of the rotorcraft is a formidable challenge and is the focus of this work. It is the key issue that needs to be overcome in order for the single pilot automated NOE capability to be practical. In particular, the ability of passive systems to obtain a sufficient approximation to dense range maps for obstacle detection within the limits of resolution and quantization, should be determined. Once the limitations of passive ranging have been determined, other active ranging methods can then be used to augment passive ranging. The difficulty arises in selecting an automatic obstacle detection technique that is dependable and robust under various scenarios such as day/night/adverse weather conditions and can be implemented and interfaced with the pilot/rotorcraft system without unduly excessive size, power, and weight demands on the rotorcraft [26, 28, 39]. The technique must also have graceful degradation, instead of total failure, under conditions of limited operability. Moreover, the detection technique should preferably be covert to minimize the threat to the rotorcraft and the pilot.

Several automated techniques for obstacle detection during land-based navigation have recently been developed. However, there are multiple factors that prevent direct application of these obstacle detection methods in the navigation of airborne vehicles. In the land-based case, search for obstacles is primarily confined to the part of the visual field (of the on-board sensors) that corresponds to the road along which the vehicle is traveling. In contrast, there is no single flight corridor for an airborne vehicle, specially for a rotorcraft in low-altitude flight. The search for obstacles, therefore, has to be performed over the entire visual field in the case of the rotorcraft. The difference in speed between a land-vehicle (top speed ~ 15 m/s) and a rotorcraft in NOE flight (top speed ~ 40 m/s) demands significantly faster data acquisition and processing rate for the latter. Since even a small obstacle like a wire could be fatal to a rotorcraft and such obstacles could lie anywhere within the visual field, the sensor resolution and the FOV are critical parameters. Note that increasing the resolution increases the required processing speed. A land vehicle has limited maneuverability, viz., the primary motion is in the longitudinal direction (direction of travel). A rotorcraft, on the other hand, very often needs to engage in longitudinal, lateral, and vertical maneuvers. Any maneuver other than longitudinal causes sudden change in the gaze direction of the sensors thereby bringing completely new objects (potential obstacles) within the visual field. Selection of appropriate FOV for the sensors and prediction of obstacles based on

the current FOV analysis are, therefore, important considerations for the rotorcraft scenario [20].

The existing methods for passive detection of obstacles are based on passive ranging and feature-based spatio-temporal analysis of TV imagery. Unfortunately, most of these methods have extremely unrealistic constraints imposed on the image formation process to make them work. The biggest sources of problems are due to sensor motion and incomplete/ambiguous information in the sensed data (imagery). Also, many of the techniques have not been developed for day/night sensors such as FLIR. Active sensors such as millimeter wave [1] (MMW) and CO_2 laser radar can detect obstacles but the continuous operation of these sensors betrays the rotorcraft covertness.

This paper describes a *maximally passive* system for obstacle detection that can improve the safety of rotorcraft during NOE flight. In Section II, we review the related research related to obstacle detection using both passive and active sensors. Section III discusses the requirements demanded of an obstacle detection and avoidance system for rotorcraft performing NOE flight. It provides the sensor suite options for different rotorcraft maneuvers. It discusses system tradeoffs when these requirements are in conflict and provides analysis for the sensor suite selection. Based on this analysis Section IV presents an innovative maximally passive approach for obstacle detection. In Section V, we present the results of an implementation of our obstacle detection system that uses outdoor imagery coupled with inertial data. Finally, Section VI presents the conclusions of this work.

II. EARLIER RESEARCH

A. Obstacle Detection Using Passive Sensors

Obstacle detection (for both autonomous land vehicles and rotorcraft) using passive sensors rely on two fundamental techniques for ranging: binocular stereo and motion stereo. Binocular stereo employs two laterally displaced sensors. These stereo methods have been widely studied for determining range passively [5, 6, 36]. In order to use binocular stereo, feature matches must be found between the two images. Once feature correspondences in the two images have been established, the range to the corresponding world points can be computed using the knowledge about the relative position/orientation of the two sensors and their internal parameters. To a first approximation, the error in binocular stereo range measurements is directly proportional to the positional error of the matches and inversely proportional to the length of the baseline [5] (lateral displacement between the sensors). However, the longer the baseline is, the more difficult it is to ensure that a large number of points are visible in both images simultaneously.

Motion stereo utilizes one sensor in motion from which image frames are collected at fixed intervals of time [2, 30]. By observing the amount of image plane-motion that a particular world point exhibits between frames (i.e., optical flow) and using knowledge of sensor motion, range to the world point can be computed. The estimation of the optical flow can be based on the derivatives (gradients) of the image brightness function when suitable constraints are applied to the flow field [29]. One fundamental limitation of these gradient-based methods is that they are highly sensitive to noise. Furthermore, theoretical analysis has shown that there is a direct conflict between various constraints imposed on the flow field [32]. In particular, it is shown that errors due to instability of solutions of the required systems of equations are inversely related to the size of the neighborhood used for flow smoothness constraints. However, increasing the size of the neighborhood violates the flow smoothness constraint.

An alternate approach to the estimation of optical flow is to match image features (points, edges, regions, or boundaries) between a temporal sequence of two or more images [6, 7, 12, 13]. The motion between frames can be decomposed into translational and rotational components. The final (usually the second) image in the sequence can then be derotated to achieve a relationship approximating pure translation between the first and final images. In the case of pure sensor translation in a stationary environment, every point seems to expand from one particular image location termed the *focus of expansion* (FOE). If the location of the FOE is known, then the relative depth of matched stationary image points can be found. If, in addition, the velocity of the sensor and the elapsed time between frames is known, then the absolute range can be computed using trigonometric formulas. This method yields relatively sparse set of points for which range values are obtained unlike the gradient-based method which yields dense set of points. However, range to other image points can be estimated using interpolation procedures. Accurate range estimates utilizing the above approach require long displacement vectors. Issues raised here include accurate frame-to-frame correspondence, accurate FOE location, and the magnitude of interpolation ambiguities.

Although the aforementioned techniques comprise the majority of methods used in passive ranging, various other approaches [31] have also been suggested. Bowman and Gross [18] have developed a method for passive ranging to targets using data from two different aircraft, which is not applicable to the rotorcraft low-altitude flight scenario. Techniques based on Kalman filtering have also been developed for general motion and passive ranging [46, 47].

B. Obstacle Detection Using Active Sensors

The two most commonly used mechanisms for active ranging are laser and MMW radar systems. Currently a number of 3-D laser scanners using phase detection technology are available [8, 42]. One such sensor, developed for autonomous vehicle navigation, has a FOV of $\pm 40°$ horizontal which covers depression angles from 15° to 45° with a range resolution of 8 cm. More advanced systems with multiple lasers operating at multiple frequencies in the visible, near infrared, and shortwave infrared wavelengths are also under development. The multiple wavelengths allow for range and reflectance determination with a $60° \times 80°$ FOV and a range resolution of 2 cm. Another commercially available 3-D laser ranging system with a $60° \times 60°$ FOV has similar range resolution. It allows a fixed pattern radar scan with 128×128 pixel resolution and a frame rate of 0.8 s. Both of the above mentioned systems have phase wrapping ambiguities on the order of 40 ft in their range measurements. Dunlay and Morgenthaler [22, 23] detect obstacles for an autonomous land vehicle navigating along a road. The range data that is processed is provided by a radar sensor which covers a $80° \times 30°$ FOV with 256×64 array of pixels (the sampling density is not sufficient for wire detection). Current attack rotorcraft possess Doppler radar navigation systems for flight guidance and laser range finders for ranging to points of interest, but these systems are not capable of imaging functions.

A compact MMW radar system has been developed which uses a 3 s scan over a 90° sector to detect obstacles or hazardous objects [1]. Prototype systems have detected 3 mm diameter high tension cables at ranges of 1000 m in foggy weather. The system is designed to detect similar objects with small cross sections. Acoustic sensors have been used for obstacle detection for land vehicle applications [21, 48].

In general, lasers and MMW radar systems are able to detect and accurately determine the range to terrain obstacles. Studies have demonstrated that both kinds of systems can successfully detect transmission cables at all angles, polarizations, and surface conditions, although transmission line detection at all aspect angles with a MMW sensor requires scanning [3]. This study was conducted using four MMW frequencies (18, 34, 56, and 94 GHz), two laser wavelengths (10.6, 1.06 μm), three polarizations (horizontal, vertical, and cross), various surface conditions (dry, wet, rough, and smooth), five kinds of cables, and several aspect angles. (For further comparison of Laser and MMW radar sensors, see Section IIIC.) Recent advances in CO_2 laser technology have led to the development of fieldable LADAR system that can provide high resolution imagery suitable for automatic target recognition [11].

Unfortunately, active systems are subject to automatic detection. They undoubtedly provide good obstacle detection capability at the price of increased danger to the crew and the vehicle, regardless of whether the active system is based on laser or MMW radar ranging. Consequently, their use should be contingent on the capabilities of passive obstacle detection/avoidance technology in near and far future systems.

III. REQUIREMENTS FOR AN OBSTACLE DETECTION SYSTEM

A. Rotorcraft Maneuvers

A rotorcraft can engage in three different kinds of maneuvers during NOE flight: longitudinal, to decelerate to a quick stop; lateral, to go around an obstacle; and vertical (*pullup* and *pushover*), to go over or under an obstacle. Besides, it may need to turn corners. Maneuvers also include deviations in rotorcraft attitude involving, in particular, the aft section of the fuselage (tail rotor). The position of the tail rotor in relation to obstacles is important, as a tail rotor strike could result in an uncontrollable spin. If data about the presence of obstacles near the tail rotor are lacking or problematic, turns during NOE flight is constrained to half flying and half pedaling the rotorcraft through a lateral turn, rather than pivoting on an axis. This requirement not only constrains the natural capabilities of the rotorcraft, but also it forces a forward motion around corners.

The main considerations that need to be accounted for during the NOE flight are, 1) to avoid obstacles on all sides of the rotorcraft and some nearby obstacles (overhanging branches); 2) to minimize or avoid hazards, such as vertical pull ups when lateral movement is possible, the use of active sensors, and the adverse effects of downwash; and 3) to move as rapidly and safely as is possible.

In the wire and wire-like object detection system (WWLODS) study [45], twenty-five Army helicopter pilots were interviewed to obtain reasonable values of the following key variables: vertical FOV (VFOV), lateral FOV (LFOV), ground clearance (Δh), helicopter airspeed (V), response time (T_R), frame time (T_F), rotor tilt angle (θ_T), climb angle (θ_c), ground slope (θ_g), and bank angle (θ_B). These pilots included seven scout (OH-58), nine attack (AH-IS), five utility (3 UH-1, 2 UH-60), and four transport (CH-47) pilots. The results of this study are summarized in Table I, where μ and σ are mean and standard deviation, respectively. The requirements for a minimum FOV were obtained by asking the pilots to define the minimum height and width of a clear window through which they would be willing to fly, and the minimum range at which they would be able to accept and use active scanner information. A number

TABLE I
Summary of WWLODS Study

Variable	Value
VFOV	15° (min)
LFOV	24° (min)
Δh	μ = 2 ft, σ = 3 ft (min); μ = 4 ft. σ = 4 ft (max)
V	0 (min); μ = 80 kts. σ = 50 kts (max)
T_R	μ = 2.5 sec, σ = 1.25 sec
T_F	<= 2 sec
θ_T	40° (nominal), 60° (possible)

of pilots expressed an interest in flying with their skids in the grass or in the treetops as well as making wire fences, barbed wire barriers, tree stumps, and the ground itself especially relevant obstacles. Some pilots expressed a desire to traverse open spaces at speeds from 160 to 190 kt, the point being to move as fast as possible, even in NOE flight. The results shown in Table I are very approximate, with large standard deviations. Later, we discuss several other constraints that considerably enlarge or in various ways complicate these values.

The frame time, during which processed frames are used to update the input of the navigation and guidance system rather than the pilot, is of primary importance in autonomous systems. We therefore define three different frame times, one for each type of range sensor under consideration: T_{FAM} is the frame time for *motion-based ranging*; T_{FAS} is the frame time for *stereo-based ranging*; and T_{FAA} is the frame time for *active ranging*. The rotor tilt angle determines rotorcraft deceleration relevant to a longitudinal stopping maneuver such that the longitudinal deceleration is $a_l = g \tan\theta_T$, where g = acceleration due to gravity. The climb angle is relevant to pull-up and pushover (push-down) maneuvers and is an unspecified function of the pull-up load factor (UPLF) which is nominally $1.5g$ (where, $1.0g$ corresponds to straight and level flight), with possible vigorous maneuvers up to $2.5g$ to $3g$. Push-down load factors (DNLFs) are nominally $0.0g$ and can be extended to $-0.25g$ to $-0.5g$ in extreme cases. Now we can easily develop the equation for θ_c. Any acceleration perpendicular to the trajectory of the rotorcraft will result in a circular motion. The centripetal acceleration is $a = v^2/r$ where v = velocity and r = radius of the circle. Over a time t, the rotorcraft can be approximated as following some fraction or arc s, of this circle. With $s = vt$ and $r\theta_c = s$, we have

$$\theta_c = \frac{s}{r} = \frac{at}{v}, \qquad \text{where} \quad a = a_{\text{up}} \quad \text{or} \quad a_{\text{down}}.$$

As will be seen, θ_g, the slope of the ground, also enters into pull-up and pushover maneuvers, because in a pull-up the rotorcraft must compensate for the increased effective height of the obstacle due to an up-slope, and in a pushover, it must attempt to decrease altitude more quickly to regain concealment on a down-slope. Slopes must have equal positive and negative limits.

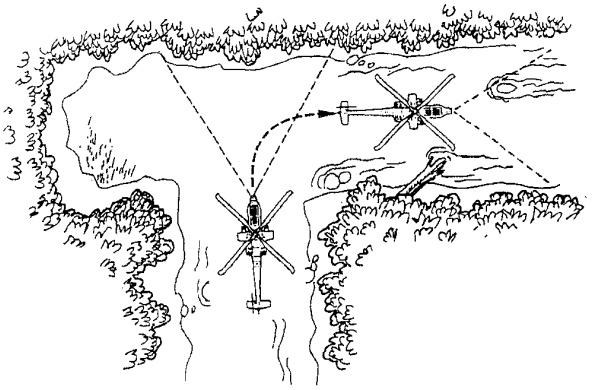

Fig. 2. As a result of narrow FOV, rotorcraft must bank to obtain complete view of surrounding environment such that safety of lateral path can be determined.

The last maneuver variable is θ_B, the *banking angle* used in lateral obstacle avoidance. Analogous to vertical maneuvers, we have $\theta_B = a_B t/v$ for lateral movement, where a_B is the banking acceleration.

Other pertinent variables which exist are processing and rotorcraft response delay (T), sensor resolution (S), number of pixels (N), and obstacle size (d). *Attitude maneuver* variables (e.g., possible angular accelerations and velocities) are not quantified since the key to avoiding collisions between the tail rotor and obstacles is an adequate knowledge of the relative 3-D positions of tail rotor and obstacle. Trajectory variables like airspeed and deceleration imply constraints on sensors and algorithms. Attitude variables do not in general imply such constraints. Consider, for example, a case in which the rotorcraft has entered an opening shaped like a capital letter T (Fig. 2). Since the passage directly in front is blocked, the rotorcraft can only move laterally, either to the right or to the left. But with a FOV at 60°, for example, it is partially blind to either side. In this case, the rotorcraft must bank to see if a lateral path is safe, rather than fly sideways. Thus, the FOV constrains attitude maneuvers and not vice versa. Consider also Fig. 3 in which the rotorcraft must make a tight turn. The banking acceleration limit is the key constraint on a tight turn. Situations like case 2 in Fig. 4, in which θ is unnaturally reduced do not arise at NOE flight velocities because the rotorcraft *cannot change heading* without the tail rotor trailing behind the rotorcraft. If this were the case, we would have to worry about the problems raised by the large disparity that would occur between frames of sensor data. But it is not the case, and again, attitude change becomes a secondary variable. Regarding constraints on attitude, the critical factors are the FOV and the sensor resolution, which delimit knowledge about obstacle location.

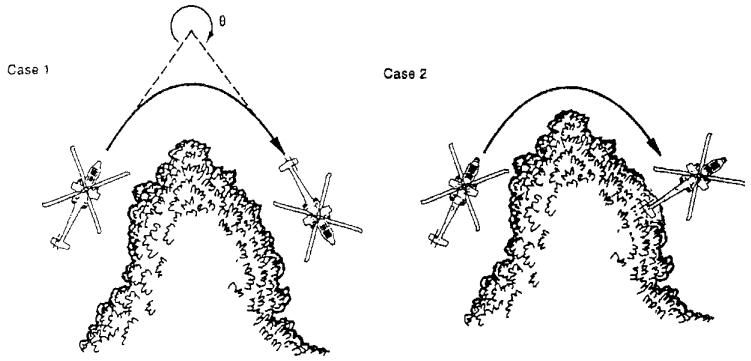

Fig. 3. When negotiating a tight turn, banking acceleration limit is the main constraint on airspeed and hence on rate of rotorcraft attitude change.

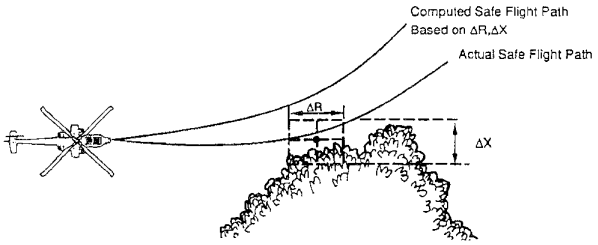

Fig. 4. Because of finite amounts of range uncertainty and spatial resolution, more conservative maneuvers must be executed. Range error ΔR and lateral position uncertainty ΔX are joined together to dictate a more conservative flight path.

TABLE II
Values of Stopping Distance R_{stop}

	Combinations of (v, a_l)			
T_{FAS}	40m/s, 1.7g	40m/s, 0.84g	20m/s, 1.7g	20m/s, 0.84g
0.01 sec	48.4m	97.6m	12.2m	24.5m
0.05 sec	50.0m	99.2m	13.0m	25.3m
0.1 sec	52.0m	101.2m	14.0m	26.3m
0.2 sec	56.0m	105.2m	16.0m	28.3m
0.5 sec	68.0m	117.2m	22.0m	34.3m
1.0 sec	88.0m	137.2m	32.0m	44.3m

B. Maneuver Imposed Requirements

1) *Longitudinal Maneuvers*: The key factor in longitudinal maneuvers is the *sensor resolution* required for obstacle detection. The sensor resolution must be sufficiently high to allow for the detection of an obstacle. Objects that fill only one pixel cannot, in general, be detected because of blurring and low signal-to-noise ratio. Depending on the scene background, contrast, and noise, anywhere from 2×2 to 5×5 pixel coverage on the object is needed. Linear objects like wires or moderately straight branches are an exception in that one pixel in the transverse axis is often sufficient for recognition, given many pixels or coverage along the wire or the branch.

It is important to note that the longitudinal stopping maneuver becomes necessary only when the environment traps the rotorcraft, i.e., disallows lateral or vertical maneuvers. Objects of pixel size (twigs, branches, and the like) are attached to larger objects and do not float freely in space blocking the path of the rotorcraft. However, wires can easily block the path of a rotorcraft and under some circumstances demand a full stop. Consequently, the ability to obtain up to 5×5 pixels on an isolated obstacle is not a requirement for longitudinal stopping whereas obtaining $l \times n$ pixels on wires is an important requirement. For instance, the stump of a small tree (say, only 5 cm in diameter) may not be detected soon enough to allow a full stop, but that is irrelevant if a slight vertical maneuver can compensate in time. If the stump is (say) a meter high, then $l \times n$ pixels will probably suffice for detection. We use the qualifier *probably* because in FLIR imagery the apparent temperature of a given obstacle may, under some circumstances, virtually match its surroundings and make detection more difficult. This means we would, in a conservative approach, gather FLIR data of critical, small obstacles to overcome detection difficulty. For the time being, we assume that $l \times n$ *pixels are sufficient for detection of small obstacles or wires* when considering the longitudinal stopping maneuver. It is to be noted that the $l \times n$ pixel criterion places severe demands on a wide FOV passive system.

To estimate the typical sensor resolution for obstacle detection during longitudinal maneuvers, we adopt the WWLODS specification [45] of maximum velocity of $v_{\max} = 80$ kts ≈ 40 m/s and a nominal velocity of $v_{\text{nom}} = 40$ kts ≈ 20 m/s. The stopping range, R_{stop}, based on the maneuver variables described in Section IIIA is given by

$$R_{\text{stop}} = \frac{v^2}{2a_l} + vT_{\text{FAS}}.$$

We assume the following values for the longitudinal acceleration parameters: $a_{l\,\text{modest}} = 0.84g$ and $a_{l\,\max} = 1.7g$. Using these nominal and maximum values, we compute R_{stop} for different values of T_{FAS} (Table II).

Table II indicates that the processing time T_{FAS} begins to have a significant impact on the stopping range beyond 0.1 s (which is a reasonable, nominal value). At a casual 20 m/s velocity, an extreme deceleration will halt the aircraft in about 14 m. Given that a certain amount of time is required to tilt the main rotor to induce a deceleration, this is probably closer to 20 m (ideally one should integrate a_l over time, but given the range of possible a_l and v values, this becomes a secondary consideration). At the other extreme, a high 40 m/s velocity coupled with a modest $0.84g$ deceleration will require over a hundred meters to stop. For nominal flight, nominal deceleration, a conservative factor for integrating a_l, and a safety margin (stopping several meters in front of an obstacle), a stopping range of $R_{stop} = 40$ m is reasonable.

The angular resolution δ is given by $\delta = d/R$ where d = obstacle size. With $R = 40$ m, and $d = 3$ mm (for 1/8 in wire), the resolution is $\delta = 0.075$ mrad ($= 0.0043°$). With a high resolution sensor (1024×1024 pixels) and FOV $= \delta N$, N being the number of pixels along one axis, the FOV would have to be less than 4.4° to obtain sufficient resolution to detect 1/8 in wires at 40 m. In a recently completed obstacle avoidance system (OASYS) study [20], it was found in working with simulations and pilots that a FOV of $20° \times 30°$ could be used to detect (1 in diameter wires at 400 m for contour flight at 80 kt) and warn pilots about the presence of obstacles.

2) *Lateral and Vertical Maneuvers*: FOV dimensions are the key consideration in both lateral and vertical maneuvers. There are two important FOV configurations: static, in which FOVs are fixed because the sensors are rigidly attached to the rotorcraft; and gimballed, in which FOVs are flexible because the sensors are mounted on gimbals. A gimballed configuration is valuable when a maneuver is anticipated. In this configuration, the sensor is pointed in the direction of the lateral or vertical acceleration to obtain a better survey of the obstacles lying in the region of the expected trajectory. The key question in determining the system requirements for lateral and vertical maneuvers is, how to infer about the peripheral objects when every sensor has a limited FOV.

To address the above question, there are three possible options. The first option is *knowledge based*, i.e., one can only trust what one knows. Suppose the obstacle detection system employs a low resolution wide FOV passive sensor and a high resolution narrow FOV active sensor, and no wires are observed by the narrow FOV active system. Hence, a knowledge-based conclusion will be the absence of wires. In reality, there may still be unseen wires outside that narrow FOV missed by the wide FOV passive system because of its low resolution. Thus, this option does not guarantee that the rotorcraft may safely maneuver into areas in the peripheral FOV. The second option is *inference based*, i.e., one can always trust what one infers. For example, detecting and ranging to wires in a narrow FOV allows a reasonable and cautious inference of their presence outside the FOV. Not detecting wires in a narrow FOV may imply their absence in the FOV periphery. The presence of towers, posts, poles, etc., in any part of the system FOV is a trustworthy indicator of the presence of wires. The final option is *context based*, i.e., the confidence one has in an inference is a matter of context. This is the most reliable option. In some scenarios valid inferences can be drawn, in others their truth is only probable. For example, in an open clearing, the absence of telephone poles, posts or towers (as determined by a wide FOV passive sensor) dependably indicates the absence of wires throughout the wide FOV.

We assume the use of a contextual option. Under this option, the changes in the obstacle avoidance trajectory will have to be made at times based entirely on direct knowledge from a narrow FOV and at other times based on knowledge over the whole wide FOV.

There are several variables which serve to constrain the extent of lateral and vertical motion maneuvers. 1) *Broad trajectory*. It is important to know in advance the location of obstacles over as broad a FOV as possible, especially to take advantage of the lateral maneuverability of the rotorcraft. 2) *Obstacle avoidane*. Due to finite spatial resolution and finite range accuracy, the 3-D positions of obstacles are uncertain. With large 3-D uncertainties, the maneuvers must involve either larger banking and climbing accelerations or lower velocities or some combination. Fig. 4 illustrates the effect of 3-D uncertainties on the conservativeness of possible maneuvers. 3) *FOV dimensions*, and 4) *Rotorcraft acceleration limits*. The first constraint requires as large a FOV as possible (even for the narrow, active FOV). The second constraint leads to a small, high resolution FOV for high range accuracy. The third constraint encourages a large FOV, and the fourth constraint restricts how large the FOV needs to be.

We assume a nominal lateral or vertical acceleration of $0.5g$, consistent with the UPLF as described in Section IIIA. Recall that the centripetal acceleration is $a = v^2/r$. So, with a nominal velocity of 20 m/s, r is greater than 80 m. In Fig. 5 we illustrate a $0.5g$ lateral maneuver around an obstacle located at a distance of 49 m. In this case, we add a displacement of 4 m attributed to a 0.2 s processing and control delay. Note that an obstacle having diameter of 10 m is accommodated in this case, allowing room for a small safety margin. The minimum avoidance distance of 49 m is greater than that required for longitudinal stopping maneuvers because of the low

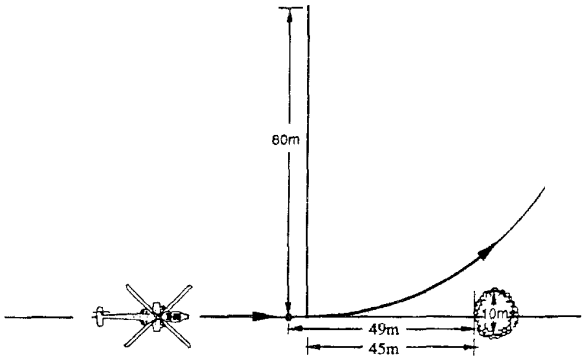

Fig. 5. Illustration of $0.5g$ lateral maneuver around an obstacle at 49 m with rotorcraft traveling at velocity of 20 m/s. The 4 m lag that occurs before turn is due to 0.2 s processing and control delay. As illustrated, clearance of tree is achieved. Note that rotorcraft is not to scale. Rotor diameter is taken as 14.63 m.

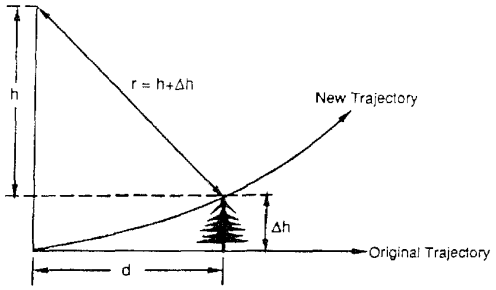

Fig. 6. Basic geometry of vertical maneuver.

lateral acceleration that was used in the calculation. Although, if, for example, a small isolated obstacle lies in the path of the rotorcraft, it is more easily avoided by a lateral maneuver than by a stopping maneuver.

A vertical maneuver will, in general, require a higher acceleration or lower velocity to accommodate a tree, partly because of the larger vertical dimensions of trees, partly because in NOE flight the rotorcraft is at an altitude of 2 to 4 m, and partly because the ground slope sometimes increases, thus giving the obstacle a greater effective height (rotor blade length is not a problem in vertical maneuvers). The basic geometry for vertical obstacle avoidance is illustrated in Fig. 6. The following relations hold (assuming a 4 m displacement during processing):

$$r^2 = h^2 + d^2, \qquad h + \Delta h = r, \qquad \text{and} \qquad r = \frac{v^2}{a}$$

from which we can derive

$$\Delta h = \frac{v^2}{a} - \left[\frac{v^4}{a^2} - d^2\right]^{1/2} = r - (r^2 - d^2)^{1/2} \qquad \text{and}$$

$$r = \frac{d^2 + \Delta h^2}{2\Delta h}.$$

For instance, with $d = 36$ m, $a = 0.5g$, $v = 20$ m/s, we find that $\Delta h \approx 8.4$ m. The variable Δh is the allowed total obstacle height plus the rotorcraft height.

For a vertical maneuver, we must also account for the ground slope θ_g which contributes an amount $\Delta h_g = d \tan\theta_g$ to the effective obstacle height. Thus,

$$\Delta h_{\text{total}} = \Delta h + \Delta h_g = r - (r^2 - d^2)^{1/2} + d\tan\theta_g.$$

Assuming a worst case slope of $\theta_g = 8°$ (up from the ground plane), $d = 36$ m, and $\Delta h_{\text{ob}} = 10$ m (e.g., a tree), we obtain $r = 50.6$ m. With $v = 20$ m/s this requires an acceleration of 7.9 m/s^2 ($\approx 0.8g$), which is large but not beyond the capability of rotorcraft. Down slopes are much easier to handle.

Errors in obstacle location have a minimal adverse affect on these numbers. Even with a 120° FOV, 512 pixels yields 0.23°/pixel ($\approx$ 4.1 mrad/pixel) which amounts to only a 0.16 m range error for a range of 40 m that is much less than ordinary obstacle dimensions. Actually, 0.16 m/pixel at 40 m may imply the need for a higher resolution (1024 pixel) sensor, since 16 cm/pixel may not be sufficient to detect many small unleaved branches and posts.

Errors in range have a larger impact on acceleration. For the vertical maneuver, a range error of $\Delta d = 3$ m will change Δh from 9.4 m to either 7.1 m (which is worse) or 10.2 m (which is better). Still, a high resolution (1024 x 1024), wide FOV stereo sensor or moderate resolution (512 x 512), narrow FOV stereo sensor will provide range error values less than 2 m, as well as resolution sufficient for detecting posts and smaller branches.

3) *Turning Corners*: The FOV must be large enough to see obstacles that lie along any curved trajectory resulting from a lateral maneuver. In other words, the sensor must be able to see every place that possible (immediate) maneuvers can take the rotorcraft, otherwise, rotorcraft maneuverability will be wasted. This FOV will be necessary when the system cannot anticipate which way the rotorcraft will maneuver. Such situations occur when the rotorcraft comes out of a narrow gap into a wide opening or when it takes a corner. In these situations it does not matter whether one has a static configuration or a gimballed configuration, because a gimbal uses the anticipation of a maneuver to direct the sensor and in these situations there is no anticipated maneuver, only a set of possible maneuvers.

With a stopping distance of 49 m and nominal lateral acceleration of $0.5g$, the required FOV depends upon two factors: Δx, the greatest obstacle dimension that is avoidable, and r_r, rotor radius. According to Fig. 7, the variable Δx is obtained as

$$\Delta x = r - [(r - r_r)^2 - D^2]^{1/2}$$

where $D = 45$ m, $v = 20$ m/s, $r_r = 7.5$ m, and $r = v^2/a$. Using these values, we have $\Delta x \approx 10$ m, which leads to a FOV of 25.3°.

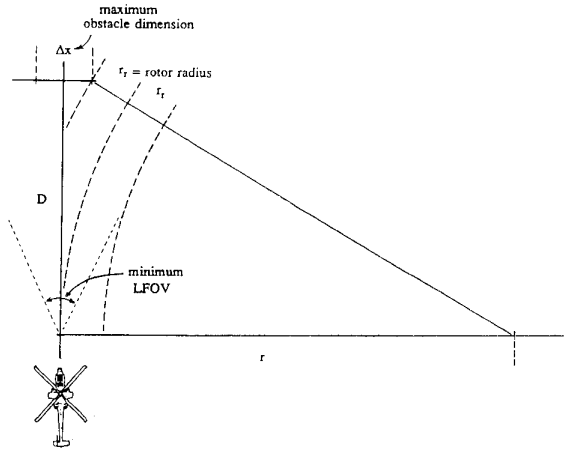

Fig. 7. Illustration of lateral maneuver where rotorcraft velocity is 20 m/s, acceleration = $0.5g$, and obstacles are detected at distance of 49 m with a 0.2 s processing and control delay. Considering rotor radius of 7.5 m, maximum object diameter is $\Delta x \approx 10$ m which requires FOV to be $\geq 25.3°$.

C. Sensor Suite Options

Motion Stereo: With a purely *motion stereo-based* system one must obtain the range to an obstacle in addition to detecting it. Since range-from-motion is not computable at the FOE (the point in the image plane corresponding to the instantaneous velocity or trajectory direction) a purely motion stereo system will fail in exactly the direction which is most relevant to the rotorcraft, and its performance will degrade severely near the FOE. Interpolation of ranges near the FOE might help, but in general, cannot be trusted. Thus, pure motion stereo-based passive ranging is not suitable by itself for *longitudinal* maneuver. The use of a narrow FOV, high resolution passive sensor would decrease the angular region of range uncertainty near the FOE and would allow for a more trustworthy interpolation of range estimates from surrounding data, but would lose important off-axis information which is crucial for *lateral* and *vertical* maneuvers.

Binocular Stereo: A *binocular stereo* system by itself, is a possibility in the sense that it can provide range estimates anywhere within the stereo FOV, but it is not a good choice for ranging to wires (for example, a very small, high resolution FOV $\sim 4°$ will be needed to detect wires 3 mm in diameter at 40 m distance). The reason is that it is difficult to solve the correspondence problem with wires because of the lack of features on these objects. Besides, other objects such as branches may occlude parts of a wire from the sensors. Because of its one-dimensional nature, the wire and the baseline of the stereo platform must not be parallel to each other so that a significant disparity may be observed in the image projections of the wire to compute the range reliably. This, in general, cannot be guaranteed. The passive ranging technique of binocular stereo is most accurate near the center of the FOV (where the FOE is located most of the time) and becomes less accurate near hte periphery. In addition, the binocular stereo approach can function even when there is no motion, e.g., the vehicle is stopped or hovering. Hence the selective use of binocular stereo is of significant utility to the obstacle detection system.

Active Sensor: In general, lasters and MMW radar systems are able to detect and accurately determine the range of terrain obstacles [35, 40, 43, 44]. For all weather conditions, a MMW radar is better suited than a laser radar. However, for terrain following, and obstacle detection and avoidance, laser radar is preferred because it is less susceptible to detection and has the necessary resolution to detect objects like thin wires (~ 3 mm at 40 m) particularly at oblique angles. However, laser scanners are not suitable by themselves because of their slow scan rate and a need for a large FOV for successful rotorcraft navigation. Overall, a laser ranging system is preferred over a MMW radar. However, the sole use of an *active system* (laser or MMW) introduces a hazardous situation and violates the philosophy of making maximal use of passive sensor technology.

Motion Stereo and Active Sensor: A combination of a large FOV *motion stereo* system and a small FOV *active sensor* can provide ranges near the FOE for *longitudinal* trajectories. A large FOV helps in thorough understanding of the scene that results in avoidance of side obstacles (including the ground), enabling of tight turns (full rotorcraft maneuverability), and increased *lateral* and *vertical* trajectory options (as it is better to move laterally than to stop or go over obstacles in NOE flight). This is the most natural option, because motion-based ranging provides its best results away from the FOE which is just what a wide FOV will provide. An active sensor with a narrow FOV will be able to detect small objects like wires near the FOE.

Binocular Stereo and Active Sensor: A hybrid *binocular stereo-active sensor* system is also possible. In theory, the binocular stereo system could range to everything but wires. It would merely detect wires during segmentation of the images. Upon detection, the passive stereo system could activate a laser to scan the wires to obtain range. To do this, a laser ranger must illuminate at least two points on the wire. These two points could also be used by the stereo system as correlation points. Such a hybrid system would minimize the use of the active component, thereby, satisfying covert operation.

Motion Stereo and Binocular Stereo: A wide FOV *motion stereo* and a narrow FOV *binocular stereo* can be combined to overcome the limitations of each approach as discussed above [17]. However, the binocular stereo component is not capable of detecting small wires. Also, joint inertial stabilization of the two laterally displaced sensors is required to

account for even the slightest vibrations that otherwise would significantly reduce (in size) the overlapping part of the two FOVs and would increase the possibility of mismatches, e.g., uncorrected vibrations (up to 1°) would lead to range errors on the order of 30%. Besides, the integrated system substantially increases the hardware and algorithm complexities.

Motion Stereo, Binocular Stereo, and Active Sensor: This is the most complex system. A large FOV motion stereo would benefit *lateral* and *vertical* maneuvers. A narrow FOV binocular stereo could be set to cover the motion-blind spot, thereby providing higher resolution (spatial and range) near the FOE than would be possible with a wide FOV stereo; thus, *longitudinal* maneuvers would be facilitated. Besides, given a narrow binocular stereo FOV that can yield fairly accurate range estimates, the active system would not be required to perform a dense scan of the FOV for obstacles other than wires, whereas, with a hybrid (motion or binocular) stereo-active sensor system only, this dense scan would be more likely.

The number of sensors in such a system becomes problematic. Four sensors are required to support the narrow FOV stereo subsystem, the wide FOV motion subsystem, and the active subsystem. Conceivably, the stereo subsystem could switch periodically from the narrow to the wide FOV, to be used for both narrow FOV stereo and wide FOV motion-based ranging. Another difficult option, setting one of the stereo cameras to a wide FOV and the other to a narrow FOV, would lose the narrow FOV resolution and thus would be ineffective. The wide FOV binocular stereo, wide FOV motion stereo, and active sensor subsystems would provide redundancy and trustworthiness. This may be absolutely necessary and not a mere luxury in the presence of low contrast, and highly occluded vegetation.

D. Tradeoffs in Sensor Suite Selection

According to the discussions in the previous section, the two best options from the standpoint of covert operation are a combination of motion and binocular stereo, and a combination of binocular and motion stereo with active sensor. We discuss these options in more detail here.

1) *Motion and Binocular Stereo*: This option involves motion-based ranging over a large FOV and stereo ranging over a small FOV centered (more or less) on the motion-blind region (FOE and its vicinity). There are several obstacles to the success of this system, despite its ostensible attractiveness. The functions of the binocular stereo component are to estimate range over the blind region and to locate wires. Earlier, we have seen that to locate wires of typical thickness (1/8 in) at typical distances (40 m) during NOE flight the FOV must be quite small (< 4° across). As a result, wires located outside the FOV remain undetected by the stereo subsystem which at the same time provides little coverage for the blind region (only 2° on either side of the FOE). One way to overcome the limitations of the binocular stereo subsystem would be to raster scan the whole stereo FOV using a 4×4 grid, for example, providing a total of $16° \times 16°$ FOV at 1/16 the original frame rate. Another option would be to employ a line scanner, 16° vertical (~ 8,000 pixels) × 1 pixel horizontal, that is set to a slow scan. Although such scanning mechanisms exist, the design of such a stereo system would require tremendous technical finesse. Finally, the binocular stereo may not be able to range to wires because of the lack of features and the relative orientation between the stereo baseline and the wires as mentioned previously.

2) *Binocular and Motion Stereo with Active Sensor*: The combination of motion stereo and active sensor employs motion-based (passive) techniques over a large FOV and covers the blind region and locates wires with a small FOV active sensor. The combination of binocular stereo and active sensor, on the other hand, uses a large stereo FOV and locates wires with a small FOV active sensor. We now discuss the relative merits of these two alternatives.

Between the two hybrid systems, the combination of binocular stereo and active sensor will provide better range information within the small FOE-centered FOV, a small plus given the presence of an active sensor. The significant difference between the systems lies in the scanning patterns of the active sensor used in each of the hybrid systems. For the hybrid motion stereo-active sensor system, the scanning pattern concentrates on the region around the FOE. Since stereo can estimate range over the FOE-centered FOV, the scanning pattern in the binocular stereo-active sensor system could be sparse that would lead to decreased detectability. On the other hand, this second binocular stereo-based hybrid system requires two sensors and possibly two inertial navigation systems (INSs) for sensor stabilization compared with one passive sensor with an INS for the former.

Another tradeoff between the two hybrid systems involves range accuracy. Assuming that the value of baseline a is known exactly, using the geometry shown in Fig. 8, the relative range error is given by [9, 10]

$$\frac{\Delta R_1}{R_1} \approx \frac{\Delta\theta_1}{\tan\theta_1} - \frac{\Delta\beta R_1 \cos\beta}{a\sin\theta_1}. \tag{1}$$

We can simplify (1) by observing that for both binocular stereo and motion stereo-based ranging, β will be small, so that $\cos\beta \approx 1$. Additionally, it may also be assumed that $\Delta\beta \approx \Delta\theta_1$ so that (1) becomes

$$\frac{\Delta R_1}{R_1} \approx \Delta\theta_1 \left[\cot\theta_1 - \frac{R_1}{a\sin\theta_1}\right]. \tag{2}$$

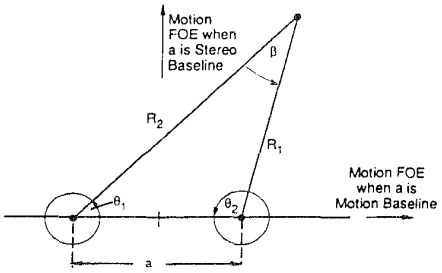

Fig. 8. Description of geometry for both motion stereo-based and binocular stereo-based ranging. Axis connecting the two spheres can represent either binocular stereo baseline or total displacement of a moving system for motion analysis.

TABLE III
The $|\Delta R_1|$ Values for Stereo and Motion-Based Ranging

	values of 'a'				
θ_1	2m	4m	6m	8m	16m
2°	87.11	41.26	25.98	18.34	6.88
5°	34.88	16.53	10.41	7.35	2.76
10°	17.52	8.31	5.24	3.70	1.40
20°	8.92	4.24	2.68	1.90	0.73
30°	6.12	2.92	1.86	1.32	0.52
40°	4.79	2.30	1.47	1.05	0.43
50°	4.04	1.95	1.26	0.91	0.39
60°	3.60	1.76	1.14	0.83	0.37
70°	3.35	1.64	1.08	0.79	0.36
80°	3.22	1.60	1.05	0.78	0.39
90°	3.20	1.60	1.07	0.80	0.40

Note: $R_1 = 40$ m and $\Delta\theta_1 = 0.004$ rad.

Note that $\Delta R_1/R_1$ is proportional to $\Delta\theta_1$ and is the largest (goes to infinity) for points along the baseline ($\theta_1 = 0$). For practical values of a, R, and θ_1, the second term in (2) dominates. Thus the magnitude of the relative range error decreases with increasing values of a. Thus, for a given FOV and pixel resolution, the binocular stereo-based relative range error ($\Delta R_1/R_1$) is maximal for points along the stereo baseline. In contrast, the motion stereo-based relative range error depends on the amount of motion and the angle away from the FOE.

To evaluate the relative accuracies of motion and stereo-based range estimates, we assume a sensor of 512 lateral pixels with a 120° FOV (the resulting instantaneous FOV or IFOV is 0.23°) and a range of $R_1 = 40$ m, i.e., $R_1\Delta\theta_1 = 0.16$ m. Thus, (2) becomes

$$\Delta R_1 = 0.16\left[\cot\theta_1 - \frac{40}{a\sin\theta_1}\right]. \qquad (3)$$

Values of $|\Delta R_1|$ computed using (3), are shown in Table III for various combinations of a and θ_1. Fig. 9 is a polar plot of the values of Table III for both binocular stereo and motion stereo-based range estimates. In Fig. 9(a), the ΔR_1 curves are drawn through points obtained from the entries in Table III (for fixed values of a). The rotorcraft is assumed to be moving towards $\theta_1 = 0°$. We observe that the ΔR_1 values rapidly increase near 0° (the FOE) for motion stereo-based ranging. In contrast, the binocular stereo-based method (with a 2 m baseline perpendicular to the motion) degrades rapidly near 0° and 180°. Recall that the ΔR_1 values are relative to an actual assumed range of 40 m.

The main impact of the range error ΔR_1 on stopping maneuvers is to make the maneuvers more cautious through reduced flight velocity. Typically, a safety margin of at least 5 m is desired even when the range is known accurately. Thus, ΔR_1 starts to impact the stopping maneuver when its value exceeds 5 m

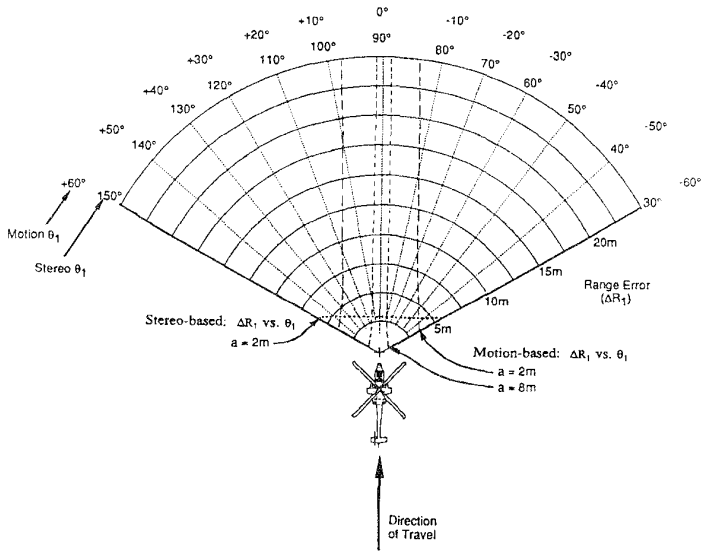

Fig. 9(a). Plot of magnitude of range error $|\Delta R_1|$ with respect to θ_1 for two different motion displacements ($a = 8$ m and $a = 2$ m) and for one value of stereo baseline ($a = 2$ m). Note that stereo-based range measurements keep ΔR_1 below 6.2 m over entire 120° FOV.

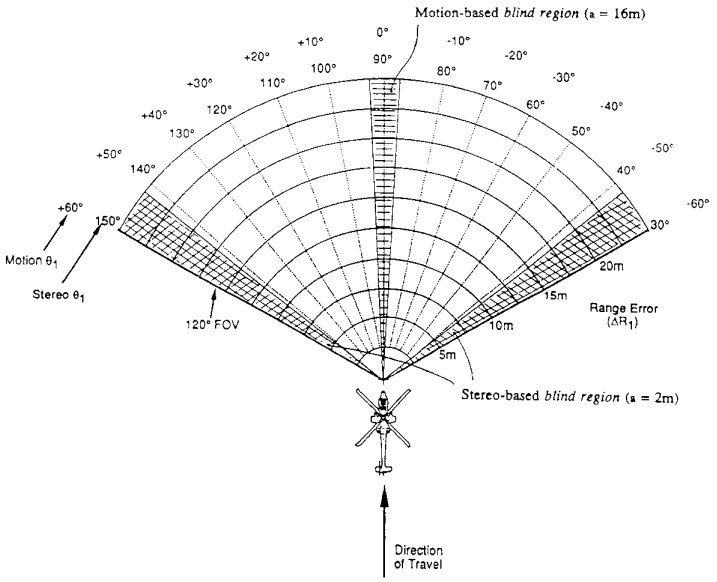

Fig. 9(b). Blind regions for motion and stereo when 5 m maximum value for $|\Delta R_1|$ is imposed.

(approximately). This definition, which is admittedly rough, serves to define the size of the blind region for motion-based ranging. From Table III or Fig. 9 we infer that for 2, 4, 6, 8, and 16 m of forward motion, the blind regions are 80°, 34°, 22°, 15°, and 5.5°, respectively. As expected, greater forward displacement reduces the dimensions of the blind region. The motion stereo-based system, however, is superior to the binocular stereo system in two ways.

First, with sufficient movement (say, 10 m or more) the motion-based range error values are very small on the periphery of the FOV. Thus, in conjunction with an active, small FOV sensor, the motion-based sensor provides smaller ΔR_1 values over the whole FOV than can be obtained with a wide FOV stereo and narrow FOV active sensor combination. If longitudinal motion dominates rotorcraft motion (rather than lateral or vertical maneuvers), it is important to note that the overall ΔR_1 values will be smaller with a motion stereo-active sensor system. Secondly, a motion-based system has the advantage of applying correspondence algorithms over successive frames rather than spatially distinct binocular stereo frames. Temporally successive frames involve smaller image displacements and offer the possibility of more robust correspondence routines. In practical terms, a motion stereo-based ranging system will probably entail fewer drop-outs and range ambiguities than a binocular stereo-based system. Note, however, there is some advantage in not depending upon motion to obtain range after the rotorcraft has navigated around a corner or has come out of some heavy clutter. This is due to the fact that motion may result in a collision while the range estimate is improving. However, sufficiently slow velocity and active scans can eliminate this problem.

3) *FOV for Sensors*: This choice is driven by many variables, the most important of which are, minimum size of detectable obstacles (d), rotorcraft airspeed (v), climb (θ_C) and bank (θ_B) angles, frame time (T_F), and pilot response time (T_R). A large FOV is preferred because it would provide for increased flexibility in trajectory when an obstacle is encountered. Unfortunately, sensor resolution must be sacrificed for FOV. Given these issues, it is clear that the obstacle detection system needs a multiple resolution sensor or multiple sensors of differing resolution. This is what leads us to the use of an active sensor.

The only way to increase FOV after a resolution has been chosen, is to increase the number of pixels in the image plane. Increasing the number of pixels will have a direct impact upon the time T_F required to process a frame of digitized imagery. This is an important consideration because T_F impacts the minimum range at which obstacles must be detected and thus the obstacle avoidance strategies.

E. Selected Sensor Suite and Its Parameters

In the following, we present the rationale behind the selection of the FOVs and resolutions of the various sensors used in the maximally passive system described in Section IV.

There are three types of sensors being used: motion stereo, binocular stereo, and laser range finder. In addition, there are two types of mountings for the various sensors: gimbal controlled orientation, and fixed orientation. We first discuss the sensors that are not gimballed.

The motion stereo sensor is used to generate a sparse range map of world features over a wide FOV. The wide FOV is required for the sparse range map

to provide suitable options for rotorcraft maneuvering when an obstacle is encountered. The binocular stereo sensor is used to provide range measurements over a medium FOV that is centered within the wide FOV of the motion stereo sensor. The purpose of the stereo sensor is to provide range samples within the area where the motion stereo measurements are the most error prone, i.e., around the instantaneous direction of vehicle heading, which lies mainly within the center of the FOV. In addition, the binocular stereo measurements can be made when the vehicle is stationary. Both the binocular and motion stereo sensors use TV or FLIR imagery to perform these measurements for day and night operations.

There are two sensors that are mounted on a gimballed platform: a variable FOV passive sensor (TV or FLIR), and a scanning laser range finder. The reason for placing the sensors on a gimbal is to allow their FOVs to constantly remain focused in the direction of rotorcraft travel, i.e., to track the FOE of vehicle motion. This is necessary considering the requirement to detect large and small obstacles (e.g., wires) which lie in the immediate path of hte rotorcraft. The laser range finder actively scans for obstacles, in a manner described below, and the passive sensor data can be used to perform motion stereo measurements or used to simply extract 2-D features which have a high probability of being obstacles (poles, wires, etc.).

An additional benefit of having gimballed sensors is that their FOVs can be directed to an alternate flight corridor when obstacles are detected in the current corridor. Reconfiguring the sensors for the alternate corridor is necessary to determine the suitability of the corridor prior to executing a change in the flight path as part of the obstacle avoidance task. The alternate flight corridors are determined from the range measurements made by the wide FOV, fixed position, sensor. In addition, the gimballed sensors can be directed to a potential landing site for the purpose of obstacle detection prior to landing. In the air vehicle scenario, the gimballed sensors can also be controlled by helmet mounted sensors.

The detection of wires and other small obstacles presents a serious problem to passive techniques because of the increased resolution required to detect such obstacles at a range sufficient for obstacle avoidance. A tradeoff must be made between the FOV and the resolution of the sensor(s). Since hte FOV of the system must be large enough such that the vehicle has sufficient (previously scanned) directions in which to steer when obstacles are detected, the FOV of the passive sensors cannot be reduced, hence a laser range scanner and an additional passive sensor with a narrow FOV are added to the system. The use of a simple (e.g., circular scanning) laser range sensor whose scan pattern is centered around the FOE, is employed for the purpose of detecting only those small obstacles

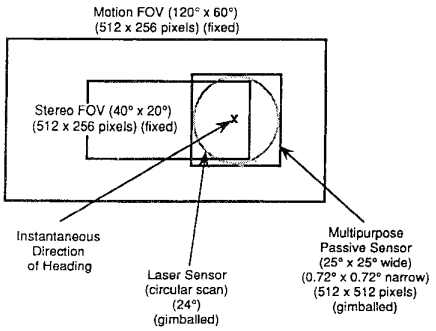

Fig. 10. Overlapping FOVs for our system.

that lie in the direction of travel. An illustration of the overlapping FOVs of the three types of sensing, optical flow, binocular stereo, and laser sensor, is provided in Fig. 10. The combination of the various sensors yields a robust obstacle detection and avoidance system. The laser sensor provides the high resolution which is not possible with a passive sensor. On the other hand, the narrow FOV passive (multipurpose) sensor reduces the density of the laser scan. The limited FOV of the laser beam sacrifices little covertness, and the simplicity of its scanning pattern keeps acquisition time short and hardware complexity low. The gimballed laser scanner can also be used to quickly investigate avenues of safe passage when obstacles have been encountered which block the current path.

Now that the purpose of each sensor has been presented, we turn to describing the parameters of each sensor. Table IV describes the parameters of each sensor. The wide FOV of the motion stereo sensor is chosen to provide a wide, cleared area in which a lateral maneuver may be performed if an obstacle is detected. The vertical FOV is half of the horizontal FOV due to the nature of NOE flight in which vertical maneuvers are not desired and lateral maneuvers are emphasized. The binocular stereo sensor has a smaller, more conventional, FOV which is centered within the motion stereo FOV.

The laser sensor scans in a circular pattern forming a cone having a 20° angle at its vertex, with a beam width of 0.5 mrad and an angular step size of 0.7 mrad (in the plane of the scan circle). This scan pattern results in 8900 range samples being acquired in 2π rad. It is important to note that, at a range of 40 m, the laser beam is 2 cm in diameter which leads to an overlap of the beam between samples. This overlap results in 4 range samples being acquired on a wire of 3 mm diameter which is perpendicular to the tangent to the scanning circle.

The laser range samples detect obstacles through a simple process. The range values are compared to a *minimum acceptable range* threshold. World points having a range less than this threshold are a danger to a vehicle. Detection of an obstacle can be confirmed

TABLE IV
Parameters of Sensor Suite

Sensor Type	Field of View	Array Size (pixels)	Instantaneous FOV (mrads)	Resolution (cm at 40m)
Motion Stereo	120° x 60°	512 x 256	4.09	16.36
Binocular Stereo	40° x 20°	512 x 256	1.36	5.45
Multi-Purpose	25° x 25° wide	512 x 512	0.852	3.41
	0.72° x 0.72° narrow	512 x 512	0.025	0.1
Laser Range	central angle = 20°	circular scan	0.5	2.0

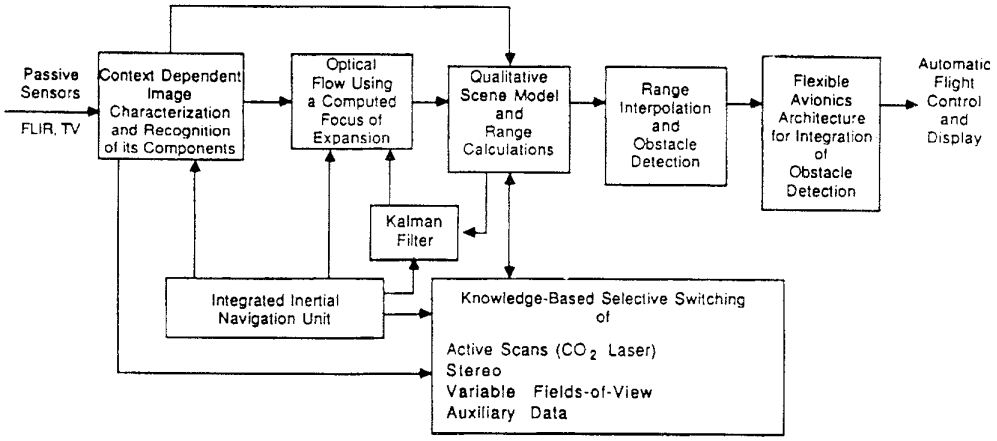

Fig. 11. INS integrated maximally passive system for obstacle detection.

with data from the passive, gimballed sensor whose line of sight is parallel with that of the laser sensor.

IV. MAXIMALLY PASSIVE OBSTACLE DETECTION SYSTEM

Based on the analysis described above, we have developed a maximally passive system for obstacle detection and avoidance. It is based upon an INS integrated optical flow algorithm and selective applications of binocular stereo and laser radar (LADAR) ranging. First, a brief description of the maximally passive system is given. This is followed by the discussions of the INS integrated optical flow algorithm.

A. System Descriptions

The schematic of the system, called ODIN, (obstacle detection using inertial navigation) is illustrated in Fig. 11. Our technique for obstacle detection and avoidance is maximally passive in that we uniquely combine data obtained from an INS into the optical flow computations. The technique also involves the use of context dependent image characterization, and the selective application of binocular stereo (passive), and laser radar (active) ranging.

An INS includes an inertial reference unit (IRU) and the necessary hardware and software to stabilize and process the IRU outputs to derive values for the platform's position and velocity of the platform in a desired reference frame [25]. IRU measurements are made with gyroscopes, to provide an absolute measure of the rotation difference between the coordinate frame of the vehicle and a fixed, geographic, reference frame; such measurements are also made with accelerometers, to provide the acceleration of the vehicle relative to the reference frame. The time integral of these accelerations gives the velocity and position of the vehicle. In addition, INS information can be used to select interest points in the visual field where range computations are to be made, and to determine sensor motion between frames [15, 41].

The incorporation of inertial data into the optical flow algorithm makes our approach robust. Traditional techniques suffer greatly from errors in the estimation of the location of the FOE and from errors in matching world points between frames. The inertial data enable our algorithm to compute (almost) the exact location of the FOE and remove the effect that sensor motion (roll, pitch and yaw) may have upon the imagery, thus the motion is effectively reduced to pure translation. When the motion consists solely of translation, the task of world point matching is greatly simplified. The end result is that more world points are assigned matches from frame to frame and the range measurements have improved accuracy.

Once the range samples are obtained from the various sensors, the next step involves obstacle

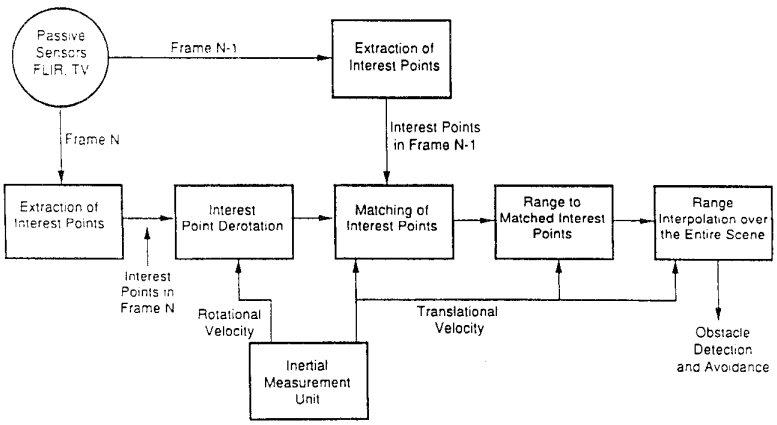

Fig. 12. Inertial sensor integrated motion analysis.

detection to be followed by obstacle avoidance. This requires that the computed range map for the scene be sufficiently dense (so as to extract the discontinuities in the range map; these discontinuities correspond to the presence of obstacles) or a model for the scene be available. By a model we mean a segmentation of the sensed image in which the various segments are labeled as different types of terrain features (sky, road, grass, etc.). Context-dependent image characterization, also called scene analysis, is applied to each frame resulting in a model of the scene which aids in the identification of safe paths and allows acquisition of dense range maps.

Having information about the scene allows for intelligent interpolation of the range values obtained with the optical flow algorithm. For example, when range values fall on two trees separated by 25 m of unobstructed space, the scene model can be used to prevent the range interpolation from connecting the trees and eliminating an otherwise free corridor between them. The result of interpolation is a more dense and accurate range map which can subsequently be used for obstacle avoidance.

B. Optical Flow-Based Obstacle Detection

To describe the details of the INS integrated optical flow-based obstacle detection algorithm, consider a given *pair* of image frames. The algorithm to estimate range values to discrete 3-D points consists of the following steps. 1) Input frames, frame A and frame B, are read in along with their associated inertial data. 2) Input images are segmented into regions corresponding to different scene entities, e.g., sky, road, tree, bush. 3) Interest points are extracted from each of the input frames. 4) Location of the FOE (in both frames) is computed. 5) FOE and the interest points in frame B are projected onto an image plane that is parallel to the image plane that captured frame A (*derotation* of frame B). 6) Interest points in frame B are matched to those of frame A based upon four criteria using various optical flow and rotorcraft motion constraints. 7) Range is computed to each interest point in frame B that has a match in frame *A*. 8) Range estimates are improved by tracking each interest point over multiple frames. A dense range map can be created using context-dependent scene analysis and interpolating between the computed range values. These steps of the algorithm are illustrated in Fig. 12 and elaborated upon in the following.

1) *Input Data Acquisition*: The input to the obstacle detection algorithm is a sequence of digitized video or FLIR frames that are accompanied by inertial data consisting of rotational and translational velocities. The inertial data together with the information about the temporal sampling interval between frames, are used to compute the distance vector $\vec{d}$ between each pair of frames and the roll, pitch, and yaw angles, (ϕ,θ,ψ), of each frame. Both $\vec{d}$ and (ϕ,θ,ψ) are crucial to the success of the algorithm.

2) *Image Segmentation*: The features within the imagery (TV or FLIR) that are most prominent and distinguished, correspond to the 3-D points to which range measurements will be made. Such points of interest are most likely to be repeatedly extracted from a long sequence of imagery. Unfortunately, not all regions within a scene can contain reliable interest points (e.g., sky or water bodies do not offer good interest points). The incorporation of image segmentation results in relatively more uniform distribution of the interest points for a given image.

Image segmentation is a two-part process. The first part, *initial segmentation*, consists of the following steps. 1) Compute the local mean "image" and the standard deviation "image" of an input image and obtain the *texture gradient* "image" using these mean and standard deviation images [16]. 2) Generate an initial binary segmentation based upon two user-specified thresholds and shrink the image so that one pixel-wide skeleton of the segmentation remains. 3) Generate a gray-level segmentation based on the multiple (user-specified) thresholds applied to the

mean images. 4) Combine gray-level segmentation results with the skeletonized binary segmentation to create a constrained edge image. 5) Link the edges in the constrained edge image to obtain the boundaries of the segmented regions. The second part, *region merging*, consists of the following steps. 1) Overlay the region boundary image on the original image and identify all the bounded regions in the latter. 2) Merge all "small" regions with an adjacent region on the basis of the size of the common boundaries. 3) Compute gray-level mean and variance for each of the resulting regions. 4) Merge regions based on similarity of gray-level mean and variance.

3) *Interest Point Selection*: We compute a set of distinguishable points by passing an operator I which is a combination of the Hessian and Laplacian operators [37] over each input frame. The operator I takes the form

$$I(g) = g_{xx}g_{yy} - g_{xy}^2 - k(g_{xx} + g_{yy})^2$$

where g is the local gray level function, and g_{xx}, g_{yy}, and g_{xy} are the local second derivatives in the x and y directions. The interest operator I actually computes a measure of gray-level curvature. In computing $I(g)$ for a particular image, the image is first smoothed by convolution with a small Gaussian kernel.

The zero-crossings of $I(g)$ are selected as interest points. Our implementation of the I operator ranks the detected interest points by the magnitude of their corresponding local maxima or *interestingness*. The interest point extraction routine takes as input a segmentation of the original image and returns n_j, $0 \leq j \leq N$, interest points in each of the N segments. The value of n_j for segment j is proportional to the segment size and other segment features. More than n_j interest points can exist per segment; only the points with the highest *interestingness* values are reported.

4) *Interest Point Matching*: Matching of interest points is the simplest if two input images differ by a pure translation between their coordinate frames, i.e., image plane B is parallel to image plane A. In this case, the FOE and pairs of interest points in frames A and B that match would ideally be collinear should the image planes be superimposed. To make the image planes parallel, derotation is performed for each vector, (F, y_i, z_i),[1] that corresponds to each of the interest points in frame B.

The matching of interest points is performed in two passes. The goal of the first pass is to identify and store the top three candidate matches for each interest point, (F, y_{B_j}, z_{B_j}), in frame B that have the smallest distance measures of all possible matches. To determine the candidate matches to (F, y_{B_j}, z_{B_j}), each of the interest points in frame A is examined with the successive use of four metrics. The *first metric* makes certain that candidate matches lie within a cone-shaped region, with apex at the FOE, bisected by the line joining the FOE and the interest point in frame B. The *second metric* requires that the interestingness of candidate matches is close to the interestingness of the point that we are trying to match. The *third metric* restricts all candidate matches in frame A to lie closer to the FOE than the points in frame B (as physical laws would predict for stationary objects). The *fourth metric* constrains the distance between an interest point and its candidate matches by imposing maximum and minimum range constraints upon the resulting match.

The goal of the second pass of the matching process is to take the matches provided by the first pass and to generate a one-to-one mapping between the interest points in frames A and B. If multiple interest points in frame B have the same best match A_i, then the point B_j, which is at the minimum distance from A_i is retained. Correspondingly, A_i appears in the list of B_j only. This process continues until all of the interest points in frame B either have a match, or are determined to be unmatchable by virtue of an empty candidate match list. In this work, we assume that the growth of objects, in terms of pixel size, for two consecutive frames due to sensor motion towards the objects is negligible.

5) *Range Estimation*: Given pairs of interest point matches between two successive image frames and the translational velocity between frames, it becomes possible to compute the range to the object on which the interest points lie. Our approach to range R computation is described by the equation

$$R = \Delta Z \frac{x' - x_f}{x' - x} \frac{1}{\cos\alpha_A}$$

where

x_f is the distance between the FOE and the center of the image plane,

x is the distance between the pixel in frame A and the center of the image plane,

x' is the distance between the pixel in frame B and the center of the image plane,

$\Delta Z = |\mathbf{v}|\Delta t \cos\alpha_F$ is the distance traversed in one frame time Δt as measured along the axis of the line of sight,

α_F is the angle between the velocity vector and the line of sight,

α_A is the angle between the vector pointing to the world object and the line of sight,

$x' - x_f$ is the distance in the image plane between (F, y_{B_j}, z_{B_j}) and the FOE,

$x' - x$ is the distance in the image plane between (F, y_{B_j}, z_{B_j}) and (F, y_{A_i}, z_{A_i}).

The range equation is used to compute the distance to a world point relative to the lens center of frame A (similar equations would compute the distance from

[1]Denotes a pixel in the 3-D coordinate frame $x - y - z$, where the image plane is located at $x = F$ and the z-axis points downwards.

the lens center of frame B). The accuracy of the range measurements that result is sensitive to the accuracy of the interest point extraction process, the matching process, and the accuracy of the INS data.

6) *Matching and Range Confidence Factors*: We further improve range computations (based upon three or more sequential frames) by predicting and smoothing the range to each interest point that can be tracked through multiple frames. The procedure for prediction and smoothing of range using multiple frames it to compute, for all interest points in a pair of images, the matching confidence, confidence in range, and predicted ranges. Once the confidences and predicted range are computed, thresholds are applied and a smoothed range is computed.

The *matching confidence* of the ith point in frame A is given by

$$C^A_{mi} = w_1\left[1 - \frac{|I_{Ai} - I_{Bi}|}{\max I_{AB} - \min I_{AB}}\right] + w_2\left[1 - \frac{|d^n_i - \min_i d^n_i|}{\max_i d^n_i - \min_i d^n_i}\right] + w_3|\hat{o}\cdot\hat{a}|$$

where $\max I_{AB} = \max_i(I_{Ai}, I_{Bi})$, $\min I_{AB} = \min_i(I_{Ai}, I_{Bi})$, $w_1, w_2, w_3 \geq 0$, and $w_1 + w_2 + w_3 = 1$. The variable I_{Xi} is the *interestingness* of the ith point in frame X and d_i is the projection of the ith point onto the line connecting its match point with the FOE. The unit vector $\hat{o}$ is in the direction of the line connecting the FOE and the ith point in frame A. The unit vector $\hat{a}$ represents the normal to the edge on which the ith interest point is located. The purpose of $|\hat{o}\cdot\hat{a}|$ is to cause the match confidence to fall when $\hat{o}$ and $\hat{a}$ are perpendicular.

The *range confidence* C^X_{Ri} of the ith point in frame X is given by the following set of equations:

$$R^0_{i\,\text{final}} = R^0_{i\,\text{predicted}} = R^0_{i\,\text{measured}} \quad \text{and} \quad C^0_{Ri} = 1 \tag{4}$$

$$R^n_{i\,\text{predicted}} = R^{n-1}_{i\,\text{final}} - \text{velocity}_i \times \text{time}. \tag{5}$$

If $(R^n_{i\,\text{presented}} \leq 0)$ then

$$R^n_{i\,\text{final}} = R^n_{i\,\text{predicted}} = R^n_{i\,\text{measured}} \quad \text{and} \quad C^n_{Ri} = 1. \tag{6}$$

Else, if $(\alpha < (R^n_{i\,\text{predicted}}/R^n_{i\,\text{measured}}) < 2 - \alpha)$ then

$$C^n_{Ri} = CM\left[1 - \frac{|R^n_{i\,\text{measured}} - R^n_{i\,\text{predicted}}|}{R^n_{i\,\text{measured}} + R^n_{i\,\text{predicted}}}\right] \tag{7}$$

$$R^n_{i\,\text{final}} = R^n_{i\,\text{measured}} + (1 - C^n_{Ri})(R^n_{i\,\text{predicted}} - R^n_{i\,\text{measured}}). \tag{8}$$

If $(R^n_{i\,\text{final}} < 0)$ then

$$R^n_{i\,\text{final}} = \frac{R^n_{i\,\text{measured}} R^n_{i\,\text{predicted}}}{R^n_{i\,\text{measured}} + R^n_{i\,\text{predicted}}}. \tag{9}$$

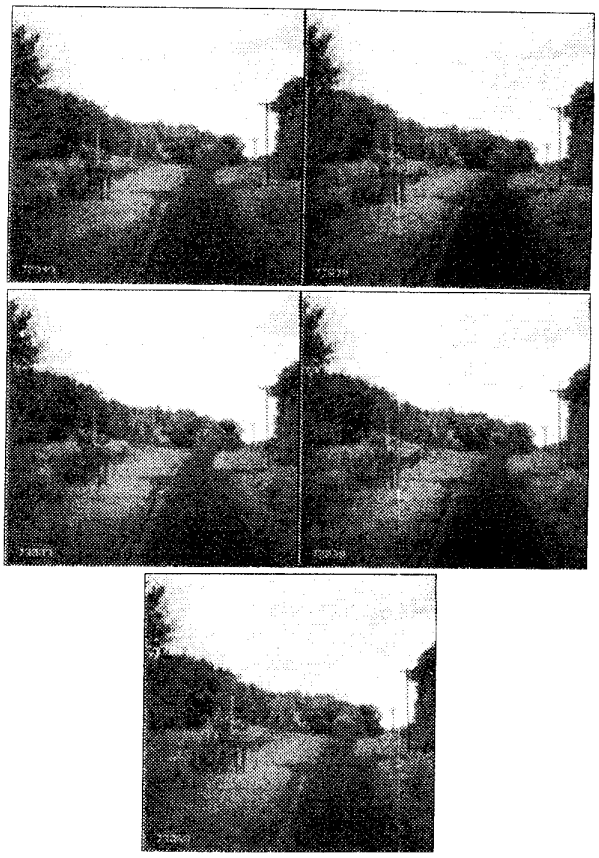

Fig. 13. Five frame sequence of outdoor imagery.

TABLE V
Actual Attitude and Velocity Measurements Made Simultaneously With Acquisition of Outdoor Imagery

Frame	Attitude (rad)			Velocity (ft./s)		
	Roll	Pitch	Yaw	v_{north}	v_{east}	v_{down}
1	3.49e-02	2.72e-02	1.33	2.24	8.36	−0.149
2	2.99e-02	2.75e-02	1.328	2.30	8.32	−0.150
3	2.61e-02	2.90e-02	1.327	2.23	8.23	−0.150
4	2.42e-02	3.01e-02	1.326	2.19	8.23	−0.120
5	2.53e-02	2.99e-02	1.325	2.01	8.23	−0.133

Note: Measurements are in coordinate frame of INS. Vehicle was moving roughly E-NE.

The variable α is a user-defined parameter that controls the range of the ratio $R_{i\,\text{predicted}}/R_{i\,\text{measured}}$.

C. Experimental Results

Our inertial navigation sensor integrated optical flow algorithm has been applied to real data (imagery and INS information) obtained from a moving vehicle to generate range samples. In this section, we present the results of applying the algorithm to two sets of outdoor imagery collected along with INS data generated by a Honeywell HG1050.

A five frame sequence of the first set is shown in Fig. 13. The FOV of the camera used to collect these

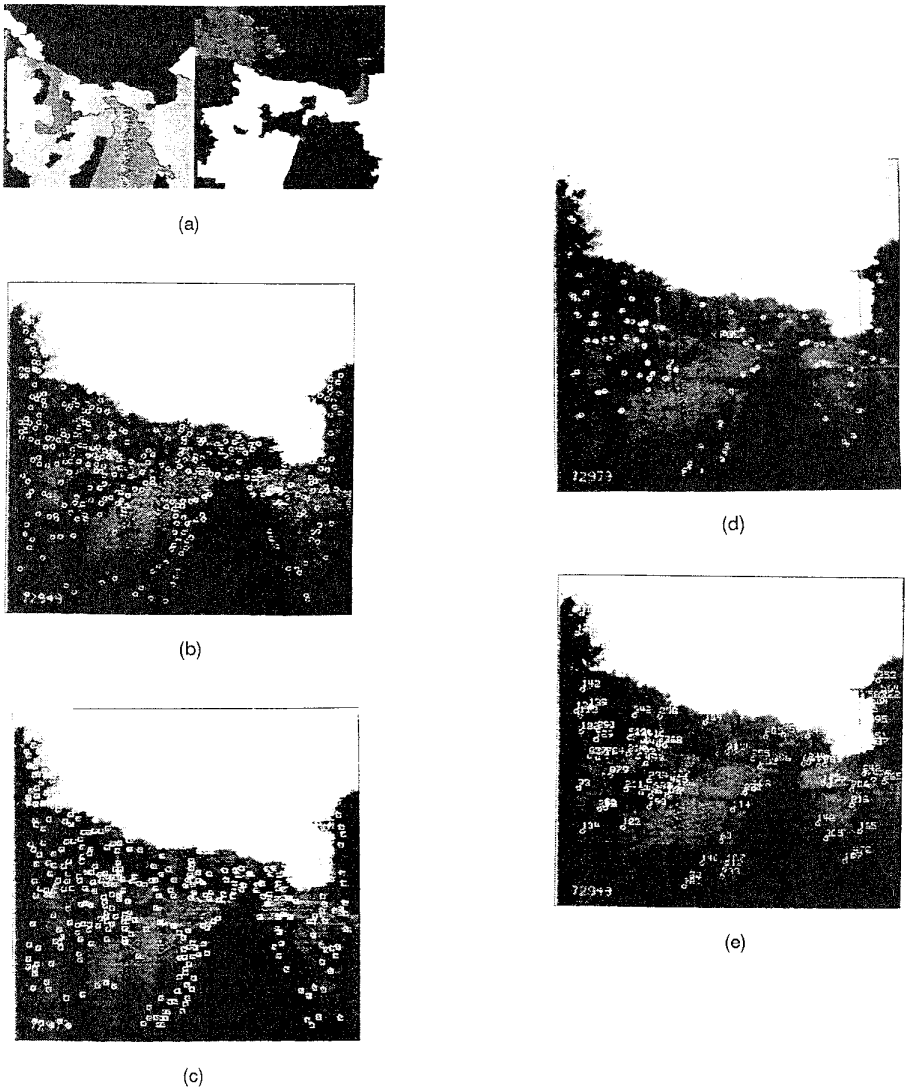

Fig. 14. Results of processing one pair of outdoor imagery. (a) Segmentation of both frames. (b) Interest points in 1st frame. (c) Interest points in 2nd frame. (d) Set of matched points. (e) Range to matched points.

images is 32.6° × 22.1° and the focal length = 15.1 mm. The elapsed time between each pair of frames for this experiment was 0.3 s. Table V indicates the roll, pitch, yaw, and velocity of the camera associated with the sequence of outdoor frames that were used. The velocity and attitude measurements are made in the coordinate frame of the INS.

The results of processing a pair of the frame sequence are displayed in Fig. 14. The image in Fig. 15 is the cumulative result of processing the 5 frame sequence. Fig. 16 shows the locations of the objects for which ground truth exists. Table VI has the comparison of ground truth range values and the range values generated through motion analysis for 4 pairs of imagery. Note that some motion analysis range values are missing because no interest points could be extracted for these ground truthed objects.

A pair of image frames from the second set of imagery is selected next. The camera has a FOV of 52.1° × 40.3° and a focal length of 9 mm. The elapsed time between the selected frames was 0.2 s. Table VII indicates the location, roll, pitch, and yaw of the camera associated with this pair. Fig. 17(a) shows the locations of the extracted interest points obtained from the first frame, drawn as circles. Similarly, Fig. 17(b) indicates the location of extracted interest points (squares) and the corresponding derotated locations (diamonds). Since the vehicle undergoes very little rotation between frames, the derotated locations are nearly coincident with the original point locations. The results of the point matching process is shown in Fig. 17(c). Finally, the computed range to each of the matched points is displayed in Fig. 17(d).

Fig. 15. Cumulative result of processing five frames of outdoor imagery. Every interest point which was matched and assigned a range is superimposed here on first frame of sequence.

Fig. 16. Locations of world points which had associated ground truth information.

V. CONCLUSIONS

We have analyzed the requirements of an obstacle detection system for rotorcraft in low-altitude NOE flight based on various rotorcraft motion constraints. We have concluded that an automated obstacle detection system for the rotorcraft scenario should include both passive and active sensors to be effective. Consequently, we have introduced a maximally passive system for obstacle detection which involves the use of INS integrated passive sensors (TV, FLIR) as well as the selective use of an active (laser) sensor. The passive component is concerned with estimated range using optical flow-based motion analysis and binocular stereo. In this work we reported the implementation of the optical flow-based motion analysis over multiple frames that is combined with INS information to compute the range to world points that lie within the FOV of the sensors. The INS integrated motion and scene analysis provides a robust passive ranging technique useful for obstacle detection and avoidance for land and air vehicle navigation. Our ongoing efforts are to complete the implementation of the remaining subsystems of the ODIN system.

ACKNOWLEDGMENTS

The authors would like to thank Banavar Sridhar and Dallas Denery of NASA Ames Research Center for their guidance and support of this work.

TABLE VI
Comparison of Grand Truth and Motion Analysis Range Values for Outdoor Imagery

Ground truth location	1–2 Range (ft.)		2–3 Range (ft.)		3–4 Range (ft.)		4–5 Range (ft.)	
	Actual	ODIN	Actual	ODIN	Actual	ODIN	Actual	ODIN
A. Telephone pole	231	185	228	276	226	245	223	202
B. Telephone pole	486	367	483	366	480	427	478	—
C. Treeline #1	502	—	499	—	497	430	494	—
D. Treeline #2	665	300	663	298	660	—	658	446
E. Treeline #4	388	—	385	—	383	255	380	—
F. Pole by gate	214	298	212	—	209	236	206	175
G. Red light post (closest to road)	153	186	150	322	148	—	145	165
H. Red light post (closest to gate)	156	167	153	343	151	114	148	157
I. Fence post by gate (west end, closest)	169	160	167	172	164	—	162	161
J. Fence post by gate (west end, farthest)	156	209	153	—	151	165	148	153

Note: Columns labeled Actual contain ground truth values and columns labeled ODIN contain motion analysis generated range.

TABLE VII
Location, Roll, Pitch, Yaw of Camera for Two Frame of Second Imagery Set

	x (ft)	y (ft)	z (ft)	roll (deg)	pitch (deg)	yaw (deg)
Frame *A*	-230.3	-20.72	6.43	0.959	-1.179	-176.737
Frame *B*	-231.7	-20.83	6.44	1.222	-1.231	-176.852

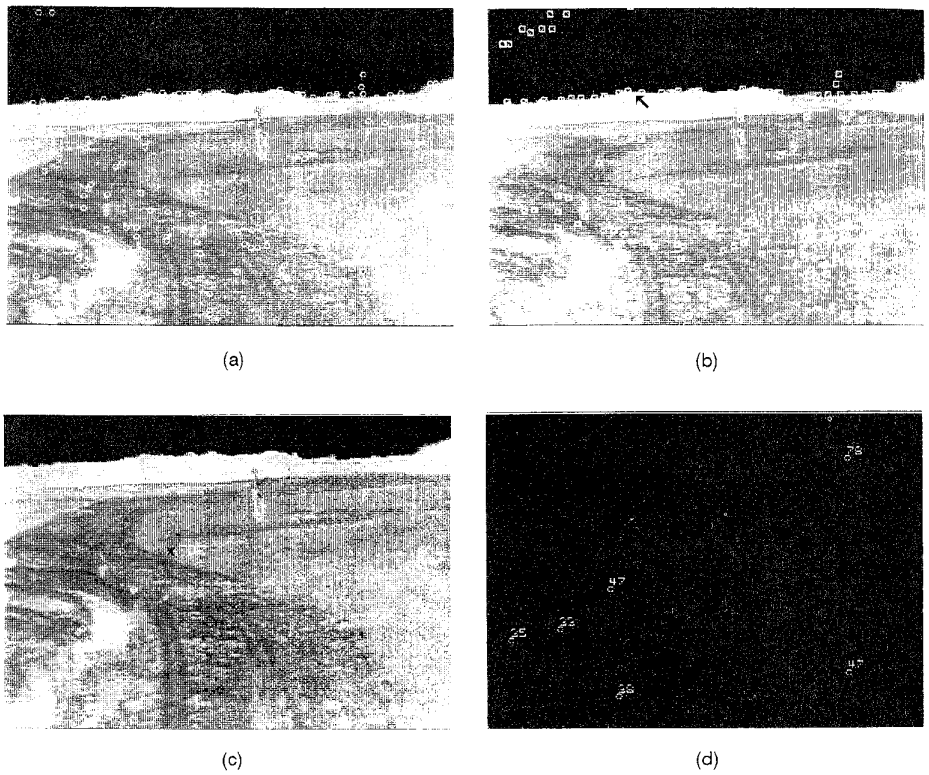

Fig. 17. Optical flow results using second set of imagery. (a) Locations of interest points in first image, indicated by circles. (b) Locations of interest points in second image, shown using squares. Diamonds indicate derotated interest point locations. (c) Matching process results in displacement vectors between circles and diamonds. FOE is indicated by a cross. (d) Computed range values to interest points.

REFERENCES

[1] Millimeter-wave radar may enhance safety of helicopter flights.
Aviation Week and Space Technology (July 1987), 103.

[2] Aggarwal, J. K., and Nandhakumar, N. (1988)
On the computation of motion from sequence of images—A review.
Proceedings of the IEEE, **76**, 8 (Aug. 1988), 917–935.

[3] Al-Khatib, H. H. (1981)
Laser and MMW backscatter of transmission cables.
In *SPIE Proceedings on Physics and Techniques of Coherent Infrared Radar* (1981), 212–229.

[4] Tuomela, C. H., et al. (1980)
Civil helicopter wire strike assessment study.
Technical report, Vols. I and II, NASA Ames Research Center, Oct. 1980.

[5] Barnard, S. T., and Fischler, M. A. (1982)
Computational stereo.
ACM Computing Surveys, **14**, 4 (Dec. 1982), 553–571.

[6] Barnard, S. T., and Thompson, W. B. (1980)
Disparity analysis of images.
IEEE Transactions on Pattern Analysis and Machine Intelligence, **PAMI-2** (July 1980), 333–340.

[7] Bazakos, M. E., and Panda, D. P. (1985)
Stereopsis and scene partitioning for terrain interpretation.
In *SPIE Proceedings on Applications of Artificial Intelligence II* (Apr. 1985).

[8] Besl, P. J. (1988)
Active optical range imaging sensor.
Machine Vision and Applications, **1**, 2 (1988), 127–152.

[9] Bhanu, B., and Roberts, B. (1990)
Obstacle detection during rotorcraft low altitude flight and landing.
Second annual technical report to NASA Ames Research Center, Oct. 1990.

[10] Bhanu, B., Roberts, B., and Duncan, D. (1989)
Obstacle detection during rotorcraft low altitude flight.
First annual technical report to NASA Ames Research Center, Apr. 1989.

[11] Bhanu, B., and Jones, T. (1993)
Image understanding research for automatic target recognition.
IEEE Aerospace and Electronic Systems Magazine, **8**, 10 (Oct. 1993), 15–23.

[12] Bhanu, B., Nevatia, R., and Riseman, E. M. (1992)
Dynamic-scene and motion analysis using passive sensors, Part I: A qualitative approach.
IEEE Expert (Feb. 1992), 45–52.

[13] Bhanu, B., Nevatia, R., and Riseman, E. M. (1992)
Dynamic-scene and motion analysis using passive sensors, Part II: Displacement-field and feature-based approaches.
IEEE Expert (Feb. 1992), 53–64.

[14] Bhanu, B., Roberts, B., and Ming, J. (1989)
Inertial navigation sensor integrated motion analysis.
In *Proceedings of the DARPA Image Understanding Workshop* (May 1989), 747–763.

[15] Bhanu, B., Roberts, B., and Ming, J. (1990)
Automatic obstacle detection and avoidance by helicopter.
In *Proceedings of IEEE International Conference on Robotics and Automation* (May 1990), 954–959.

[16] Bhanu, B., and Symosek, P. (1987)
Interpretation of terrain using hierarchical symbolic grouping.
In *Proceedings of the DARPA Image Understanding Workshop* (Feb. 1987), 466–474.

[17] Bhanu, B., Symosek, P., Snyder, S., Roberts, B., and Das, S. (1994)
Synergism of binocular and motion stereo for passive ranging.
IEEE Transactions on Aerospace and Electronic Systems, **30**, 3 (July 1994), 709–721.

[18] Bowman, C. L., and Gross, M. (1985)
Multi-sensor track association using kinematics and attributes.
In *Proceedings IEEE National Aerospace and Electronics Conference* (1985), 204–208.

[19] Burrows, L. T. (1984)
Helicopter wire strike protection system qualification testing.
Presented at the National Specialists' Meeting on Helicopter Test Technology, Southeast Region of the American Helicopter Society, Oct. 1984.

[20] Cerchie, P. H., Shipley, B. D., and Aust, R. (1989)
Obstacle avoidance system (OASYS) study.
Final report for OASYS Program, Center for Night Vision and Electro-Optics, For Belvoir, VA, Aug. 1989.

[21] Daily, M. J., Harris, J. G., and Reiser, K. (1987)
Detecting obstacles in range imagery.
In *Proceedings of DARPA Image Understanding Workshop* (Feb. 1987), 87–97.

[22] Dunlay, R. T. (1987)
Obstacle avoidance perception processing for the autonomous land vehicle.
In *Proceedings of IEEE Conference on Robotics and Automation* (Apr. 1987), 912–917.

[23] Dunlay, R. T., and Morgenthaler, D. G. (1986)
Obstacle avoidance on roadways using range data.
SPIE, Mobile Robots, **727** (Oct. 1986), 110–116.

[24] Dutta, R., Manmatha, R., Riseman, E. M., and Snyder, M. A. (1988)
Issues in extracting motion parameters and depth from approximate translational motion.
In *Proceedings of DARPA Image Understanding Workshop* (Apr. 1988), 945–960.

[25] Farrell, J. L. (1976)
Integrated Aircraft Navigation.
New York: Academic Press, 1976.

[26] Greene, D. A. (1988)
Night vision pilotage system field-of-view (FOV)/resolution tradeoff study flight experiment report.
Final technical report NV-1-26, U.S. Army CECOM Center for Night Vision and Electo-Optics, Fort Belvoir, VA, Jan. 1988.

[27] Gunston, B., and Spick, M. (1986)
Modern fighting helicopters.
In *Crescent Books* (1986).

[28] Hershberger, M. L. (1984)
Display for correlated sensor data, vol. 1, system analysis.
Technical report AFWAL-TR-84-3042, Wright Patterson Air Force Base, June 1984.

[29] Horn, B. K. P., and Schunck, B. G. (1981)
Determining optical flow.
Artificial Intelligence, **17** (1981), 185–203.

[30] Huang, T. S. (1987)
Encyclopedia of Artificial Intelligence, Vol. I.
New York: Wiley, 1987, chapter on motion analysis.

[31] Inigo, R. M., McVey, E. S., Berger, B. J., and Wirtz, M. J. (1984)
Machine vision applied to vehicle guidance.
IEEE Transactions on Pattern Analysis and Machine Intelligence, **PAMI-6** (Nov. 1984), 820–826.

[32] Kearney, J. K., Thompson, W. B., and Boley, D. L. (1987)
Optical flow estimation: An error analysis of gradient-based methos with local optimization.
IEEE Transactions on Pattern Analysis and Machine Intelligence, **PAMI-9**, 2 (Mar. 1987), 229–244.

[33] Kleehammer, R., and Hunt, J. (1979)
Wire obstacle warning system (WOWS) a real-time airborne sensor for automatic detection and recognition of wirelike objects.
In *Proceedings of SPIE Conference on Smart Sensors*, **178** (1979), 167–174.

[34] Letalick, D. (1981)
Detection of obstacles for low-flying aircraft.
Technical report from National Defense Research Institute, Linkoeping, Sweeden, Aug. 1981.

[35] Loftus, T. (1981)
Feasibility development model of an airborne CO_2 ranging sensor.
Technical report, Naval Weapons Center, China Lake, CA, Mar. 1981.

[36] Marr, D., and Poggio, T. (1979)
A computational theory of human stereo vision.
Proceedings of the Royal Society of London, **B204** (1979), 301–328.

[37] Nagel, H. H. (1983)
Displacement vectors derived from second-order intensity variations in image sequences.
Computer Vision, Graphics, and Image Processing, **21** (1983), 85–117.

[38] Potter, K. E. (1981)
Techniques for overhead-wire detection.
IEE Proceedings, **128**, Pt. F, 7 (Dec. 1981).

[39] Reago, D. A., Jr. (1989)
Azimuthal FOV requirements for helicopter obstacle avoidance sensors.
Final technical report NV-2-22, U.S. Army CECOM Center for Night Vision and Electo-Optics, Fort Belvoir, VA, Sept. 1989.

[40] Rembold, B., Wippich, H. G., Bischoff, M., and Frank, W. F. X. (1983)
A 60 GHz collision warning sensor for helicopters.
Presented at the Fifth Radar Technology Symposium, Munich, West Germany, Nov. 1983.

[41] Roberts, B., and Bhanu, B. (1990)
INS-integrated motion analysis for autonomous vehicle navigation.
In *Proceedings of the DARPA Image Understanding Workshop* (Sept. 1990), 364–375.

[42] Sampson, R. E. (1987)
3-D range sensor—Phase shift detection.
IEEE Computer on CAD-Based Robot Vision, special issue (Aug. 1987), 23–24.

[43] Schenkel, F. W., and Finkel, A. (1975)
NOTER (nap-of-the-Earth) 95 GHz radar wire avoidance system.
DARPA Technical report, Defense Advanced Research Projects Agency, Arlington, VA, July 1975.

[44] Silverman, B. B., Green, W. J., Jr., Cantor, A. J., Hoffman, N. N., Hart, R. A., and Newman, L. A. (1985)
Multifunction CO_2 NOE sensor.
Final technical report, U.S. Army Avionics, June 1985.

[45] Silverman, B. B., Heynau, H., and Mongeon, R. J. (1981)
Design approach for a laser wire and wire-like object detection system (WWLODS).
Technical report, U.S. Army Avionics, May 1981.

[46] Sridhar, B., Cheng, V. H. L., and Phatak, A. V. (1989)
Kalman filter based range estimation for autonomous navigation using imaging sensors.
In *Proceedings of 11th IFAC Symposium on Automatic Control in Aerospace*, Tsukuba, Japan, July 1989.

[47] Sridhar, B., and Phatak, A. V. (1988)
Simulation and analysis of image-based navigation system for rotorcraft low-altitude flight.
AHS National Specialists' Meeting, Automation Applications of Rotorcraft, Atlanta, GA, Apr. 1988.

[48] Thorpe, C., Schafer, S., and Kanade, T. (1987)
Vision and navigation for the Carnegie-Mellon Navlab.
In *Proceedings of DARPA Image Understanding Workshop* (Feb. 1987), 143–153.

[49] Vollmerhausen, R. H., and Nash, C. J. (1989)
Design criteria for helicopter night pilotage sensors.
Paper from U.S. Army CECOM Center for Night Vision and Electo-Optics, Fort Belvoir, VA, 1989.

[50] Warrick, P. A. (1989)
The aviation wire strike problem: The duty to warn of this aerial hazard.
Journal of Air Law and Commerce, **54** (Spring 1989), 857–887.

Bir Bhanu (S'72—M'82—SM'87—F'96) received the B.S. degree (with Honors) in electronics engineering from Institute of Technology, BHU, Varanasi, India; the M.E. degree (with Distinction) in electronics engineering from Birla Institute of Technology and Science, Pilani, India; the S.M. and E.E. degrees in electrical engineering and computer science from the Massachusetts Institute of Technology, Cambridge; the Ph.D. degree in electrical engineering from the Image Processing Institute, University of Southern California, Los Angeles; and the M.B.A. degree from the University of California, Irvine. He also received a Diploma in German from B.H.U., Varanasi, India.

Since 1991, Dr. Bhanu has been a Professor of Electrical Engineering and Computer Science and Director of Visualization and Intelligent Systems Laboratory at the University of California, Riverside. Prior to his current position, Dr. Bhanu was a Senior Honeywell Fellow at Honeywell Systems and Research Center. He has also worked with the Department of Computer Science, University of Utah, IBM San Jose Research Laboratory, INRIA-France, and Ford Aerospace and Communications Corporation. His current interests are computer vision, robotics, graphics and visualization, machine learning, artificial intelligence, and signal and image processing.

Dr. Bhanu has 5 U.S. and international patents and over 150 reviewed technical publications in the areas of computer vision, image processing, robotics, artificial intelligence and learning. He is the guest editor or co-editor of special issue of IEEE *Computer* on "CAD-Based Robot Vision" Aug. 87, *Journal of Robotic Systems* on "Passive Ranging for Robotic Systems" Sept. 92, *IEEE Trans. on Pattern Analysis and Machine Intelligence* on "Learning in Computer Vision" Sept. 94, *International Journal of Machine Vision and Applications* on "Innovative Applications of Computer Vision" Nov. 94, *IEEE Trans. on Robotics and Automation* on "Perception-Based Real-World Navigation" Dec. 94 and *IEEE Trans. on Image Processing* on "Automatic Target Detection and Recognition" (early 1997). He is on the editorial board of the *Journal of Mathematical Imaging and Vision*, the *Journal of Pattern Recognition*, and *International Journal of Machine Vision and Applications*. He is the co-author of books on "Computational Learning for Adaptive Computer Vision" (Plenum, 1996), "Genetic Learning for Adaptive Image Segmentation" (Kluwer Academic, 1994), and "Qualitative Motion Understanding" (Kluwer Academic, 1992). He has given national short courses on Intelligent Automatic Target Recognition and he is a reviewer to over 30 technical publications and government agencies. He was the General Chair for the first IEEE Workshop on Applications of Computer Vision (Palm Springs, CA, 1992) and he is the General Chair for the IEEE Conference on Computer Vision and Pattern Recognition (San Francisco, CA, 1996). He is listed in the American Men and Women of Science, Who's Who in America and Who's who in the World. He is a member of ACM, AAAI, Sigma Xi, Pattern Recognition Society, and SPIE.

Subhodev Das (S'82—M'92) received his B.Tech. (Hons.) degree in electronics and electrical engineering from the Indian Institute of Technology, Kharagpur, in 1984, his M.S. degree in electrical engineering from the University of Hawaii, Honolulu in 1986, and his Ph.D. degree in electrical and computer engineering from the University of Illinois at Urbana-Champaign in 1991.

Between 1991–1994, he was with the College of Engineering at the University of California, Riverside. Currently, he is a research staff member at PEB, Inc., Princeton, NJ, working on real-time vision systems. His research interests include intelligent systems, computer vision, machine learning, human-computer interaction, real-time computing, parallel and distributed processing, and applications of artificial intelligence, signal and image processing.

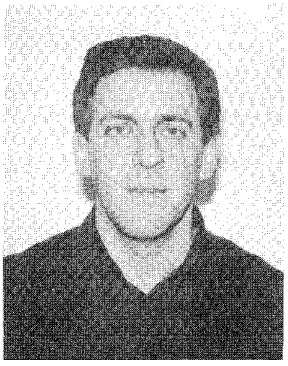

Barry A. Roberts received the B.S., M.S., and Ph.D. degrees in electrical engineering, all from Purdue University, Lafayette, IN, in 1982, 1984, and 1987, respectively.

During 1987–1988, he was a visiting Assistant Professor in the School of Electrical Engineering at Purdue University, creating and teaching the graduate level course in computer vision and performing autonomous robot navigation research in Purdue's Robot Vision Lab. He joined the Honeywell Technology Center in 1988 where he is currently a principal research scientist in the area of information processing architectures and systems. His topics of research involve the fields of signal and image processing, computer vision (e.g., passive ranging using motion stereo and binocular stereo processing), and machine learning techniques (applied to computer vision problems).

David A. Duncan received the B.A. in physics from Boston University, Boston, MA, in 1976, the M.A. in physics from Dartmouth College, Hanover, NH, in 1979, and the Ph.D. in philosophy of science from the University of Minnesota, Minneapolis, in 1990.

He joined Honeywell in 1980. During his stay at Honeywell he was responsible for algorithm development under various computer graphics, target recognition, and intelligent tracking contracts. In 1992, he became a consultant for Honeywell on technology for the disabled. He is currently working on educational projects and publications.